DTU Nanotech
Department of Micro- and Nanotechnology

DTU

Fabrication and Test of Chips for Electron Microscopy of Processes in Liquids

Bachelor Thesis. Physics and Nanotechnology bachelor program

By

Christian Fink Elkjær, s052985
Jakob Lyager Rasmussen, s052695

Nanotech, January 23rd 2009

Technical University of Denmark (DTU)

Abstract

Scanning electron microscopy (SEM) of encapsulated liquids is an interesting technology under development. It requires thin membrane penetrable to the electron beam, to separate the liquid phase from the vacuum of the chamber, and allows imaging of objects in a more real environment, for instance biological samples and chemical reactions. The aim of this project has been to create a device with a membrane like that, and additionally to include temperature and pressure sensors, a heating element and electrodes for electro chemistry, all made in a single metal layer.
This report describes the fabrication of the chip, presenting all steps of the process, including design phase, processing, test of device and to a limited extend use in SEM.
The device has been fabricated with a 50 nm thick membrane and 100 nm thick gold metal layer. With this configuration, the temperature sensor works with high accuracy, the pressure sensor is shown to work with around 0.1 bar precision, it is not functioning problem free, but at least the working principle seems to be correct. Electro chemical results has not been obtained with our chip mounted in the SEM housing, but has been performed with a chip freely suspended in electrolyte, and with a more simple chip with large electrodes for metal deposition in-situ. At the submission date, electron microscopy of liquids was performed only in a simple cell featuring just a membrane and no metal layer.
Furthermore, it has been demonstrated how AFM can be used to study the deflection of the membrane and be used to determine Young's modulus and build in stress in the membrane.
Apart from the lack of actual use of the cell in SEM, the work has in large part been concluded, and the goal of manufacturing a device with a certain set of abilities has, to a large extend, been obtained.

Preface

The present report is describing project work carried out between September 2008 and January 2009 as part of the bachelor program in physics and nanotechnology at the Technical University of Denmark, DTU.
We were specifically looking for a project at Nanotech involving cleanroom fabrication, and preferably something limited that would let us take part in all areas; design, fabrication and device testing. A chat with Kristian Mølhave convinced us that this project would allow us to do exactly that, and we therefore selected it. Something that seemed especially appealing for future researchers like us was the perspective of fabricating a device that would possibly allow us to take a (small) part in a new research field, namely electron microscopy in liquids.
Our work plays the role of a preliminary study of the area, and will be followed up by a PhD. position, and the general idea of the entire project is in large part to determine if this is even possible. How thin can you make the membranes without breaking them? Can you make a strain gauge on top of a membrane to measure pressure? Can we control the temperature in the cell? Can we do electrochemistry in the cell?
In the first part of the work, we tried to answer these questions via simulations (Comsol), calculations and literature studies, leading up to a final design idea. This design was transferred to masks and the device was fabricated in the Danchip Clean Room. For us, all of this has included a learning curve, we had no prior experience with Comsol and practical cleanroom fabrication, so an important part of the project has also been to gather experience in these areas for future use.
We would like thank our supervisors, Kristian and Torben for help, guidance and good collaboration during the last 5 months.
The work has been evenly divided between the two authors.

We hope you will enjoy reading the report.

Christian Fink Elkjær Jakob Lyager Rasmussen

Contents

1 Introduction **1**

2 Design **2**

2.1 Chipdesign . . . 2

2.1.1 Requirements . . . 2

2.1.2 The basic design . . . 3

2.2 The membrane . . . 4

2.2.1 Silicon nitride . . . 4

2.2.2 Heavy p-type doping as etch stop . . . 4

2.2.3 A first look at membranes, small deflection . . . 5

2.2.4 Large deflection, a closer look at theory of thin membranes . . . 5

2.2.5 Membrane fracture . . . 6

2.3 Simulations of membrane deflection . . . 6

2.3.1 2D model . . . 7

2.3.2 Meshing . . . 7

2.3.3 Postprocessing . . . 8

2.3.4 Results . . . 8

2.4 Pressure sensor . . . 11

2.4.1 Piezoresistivity . . . 11

2.4.2 Temperature response . . . 12

2.4.3 Proposed design . . . 12

2.4.4 Wheatstone bridge . . . 12

2.4.5 Simulations of response . . . 14

2.5 Thermistor . . . 17

2.5.1 Mask design of thermistor . . . 17

2.6 Heater . . . 18

2.7 ZIF-connection . . . 18

2.8 Final layout . . . 19

2.8.1 Window . . . 20

2.8.2 Dicing marks . . . 21

2.8.3 Electrical connections . . . 21

3 Fabrication **22**

3.1 Process . . . 22

3.1.1 Different versions fabricated . . . 24

3.2 Processing problems . . . 25

3.2.1 First batch . . . 25

3.2.2 Second batch . . . 26

3.3 Sample holders . . . 27

3.3.1 No-seal PMMA holder . . . 27
3.3.2 New generation of original holder . . . 28
3.3.3 "‘Fill-easy"’ holders . . . 28
3.3.4 Connections, the Double ZIF socket . . . 29
3.4 Yield . . . 29

4 Results **31**
4.1 AFM measurements of membrane deflection . . . 31
4.1.1 Membrane fracture . . . 32
4.1.2 Fitting to AFM . . . 33
4.2 Calibration of the thermistor . . . 35
4.2.1 Data . . . 35
4.2.2 Theory of conductance in thin metal films . . . 36
4.3 Pressure sensor measurements . . . 39
4.3.1 Test setup . . . 39
4.3.2 Chip1, strange behaviour . . . 40
4.3.3 Response at constant temperature . . . 40
4.3.4 Varying temperature . . . 41
4.3.5 Modulating data . . . 43
4.3.6 Summing up of the pressure sensor data. . . . 43
4.3.7 Another approach to simulating strain . . . 45
4.3.8 Additional thoughts on the pressure sensor . . . 46

5 Electron Microscopy **47**
5.1 SEM . . . 47
5.1.1 A brief introduction . . . 47
5.2 Pictures from wet SEM . . . 48
5.2.1 Movie of moving silver colloids in glycerol . . . 48
5.2.2 Electroplating with gold . . . 50
5.2.3 Cyclic voltammetry . . . 50

6 Outlook and Conclusion **52**
6.1 Future work . . . 52
6.1.1 The design . . . 52
6.1.2 Electrodes . . . 52
6.1.3 Transfer to TEM . . . 53
6.2 Conclusion . . . 53

7 Appendix **55**

1 Introduction

Electron microscopy is an important and widely used tool for imaging of very small structures. It has its limits though, because it takes place in vacuum, it is only possible to study dry samples, no liquids or gasses that will evaporate in the chamber. This report presents the fabrication of a Micro-Electro-Mechanical-System, MEMS, that will allow for study of wet samples in scanning electron microscope SEM. The device is separating a liquid from the vacuum of the SEM chamber with an extremely thin membrane that is transparent to electrons, and in this way image whatever is on the other side of the membrane. A system like this has been demonstrated by [Thiberge et al., 2004] using a polymer membrane, and a system for TEM was recently presented by [Creemer et al., 2008] using silicon nitride as membrane material.
The silicon nitride posses unmatched mechanical properties, it is very brittle and has a high fracture strength, and has also been the material of choice for the device presented here.
Preliminary tests of the nitride membranes had been carried out at DTU Nanotech by Kristian Mølhave with a very simple membrane chip. The goal of this project has been to make a new generation of a chip for SEM use, specifically it was desired to do electro chemistry inside the cell on the membrane, and the device should therefore have electrodes placed here. In addition to this, the chip was designed with an integrated resistive heater and a thermistor allowing for control and monitoring of temperature. Finally the design also features a pressure sensor to monitor the pressure inside the cell.
The basic idea is to make a simple design, where only one metal layer is used to create all sensors. Gold was chosen, due to it's very stable and inert properties for the electro chemistry application, but also because it is possible to deposit it with a very low stress, something that is important when it is placed on top of a very thin membrane.
The report is build around the course of events throughout the project. In the first sections, some simple simulations and calculations are presented on each sensor type. This acts as a verification of the design ideas, and is used to decide upon a final design of the chip.
After this, the process of fabrication is described, also including the problems encountered throughout this work. In addition to this, it is also described how the packaging of the device is realized, and how different designs for chip holders have been tried.
When all this work was done, measurements could be performed to test the different sensors on the chip, to see if the first calculations and assumptions were right. Since this was not always the case, the theory is expanded, to try and better explain for the observed phenomena. Hopefully these theoretical considerations and modeling presented will be of use in the future work in the field here at Nanotech.
Finally, there is a small section on electron microscopy, presenting pictures of liquid SEM of moving nanoparticles in glycerol. Unfortunately, a full electrochemical experiment in SEM with controlled temperature and pressure was never done within the time frame of this project, but the other results obtained and presented definitely bode well for the realization of this.

2
Design

2.1 Chipdesign

In the following sections the different parts of the chip design will be lined out. The word sub-device will refer to a part of the chip, e.g. the pressure sensor, whereas chip or device will refer to the entire system.
The first step of the process is to look at the different sub-devices, and provide some estimates for device behavior based on fundamental equations and simulations, and this way, hopefully provide a sound basis for optimization of the device in the future. A design was proposed according to these estimates, and a chip layout was drawn and transferred to masks and produced at the Danchip cleanroom facility.

2.1.1 Requirements

The first generation membrane chip, that was produced prior to this project, had membranes only. This second design focuses on adding sub-devices to make it a full featured electrochemical cell into which it is possible to see with an electron beam. This means that the device must be able to control and monitor temperature, must have electrodes on the membrane and a pressure sensor must be included. The role of the pressure sensor is, in addition to bringing useful information about the conditions in the cell, also to alarm in case of a high pressure that would possibly burst the membrane and endanger the microscope. This will be especially important in a future design with microchannels where there will be a flow of liquid past the membrane, and for this reason, the pressure sensor has to be situated close to the electrochemistry membrane, in order to monitor the local pressure. If this was not the case, an easy solution would have been to add a normal commercial pressure sensor somewhere in the fluidic system (though this could still be done as an addition). Since the final goal is to create a dual membrane cell usable in TEM, the chip area should not exceed 3×3 mm^2, which is the size of the TEM sample holder. On the other hand, an easy solution for connecting the chip electrically is to make it fit a so-called ZIF socket which is 8.5mm wide. In the present case, a compromise has been chosen: The area of the chip containing sensors and membrane must not exceed 3×3mm^2, but this area is on the other hand connected to bigger electrodes and thus fit into a ZIF socket. This allows ease of use during this project, but still allow for quick transfer of the design to TEM application.
To sum it up, the design requirements have been as follows:

- A silicon nitride membrane strong enough to withstand at least a 1 bar pressure difference
- Electrodes on top of the membrane with variating gaps
- A resistive heater that allows for heating of chip, liquid and housing when inside the microscope

- A termistor that allows accurate monitoring of temperature
- A pressure sensor, preferably with 0.1 bar sensitivity in the interval 1 to 2 bar pressure difference
- Area containing sub-devices (heater excluded) must be no bigger than $3 \times 3\text{mm}^2$
- Mountable in a ZIF socket for easy connection

2.1.2 The basic design

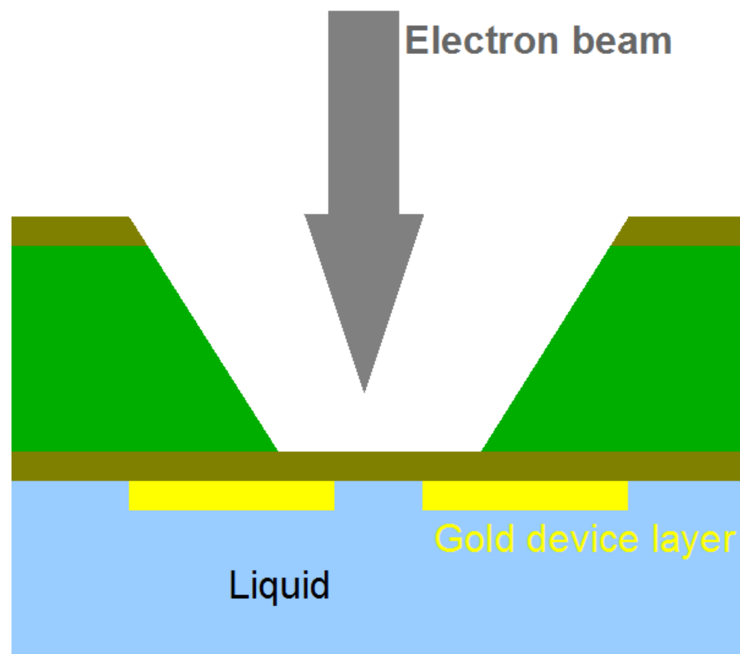

Figure 2.1: Crosssection of the chip showing the hole through the silicon, the free standing membrane and the metal layer on top. Nitride is brown, silicon green and metal is yellow. Dimensions are not correct.

To help in understanding the next sections, the basic chip design and processing will be lined out here.
For a schematic cross-section of the chip, see figure 2.1. First and foremost, a very thin ($<$100 nm) nitride is grown on both sides of a 4 inch silicon wafer. Holes are made on the backside and the silicon is chemically etched all the way through, so that the nitride on the front stands free and acts as a membrane. At the second process step, a metal layer is created on the front side, including on top of the membranes.
The metal layer will form all sub-devices, that is thermistor (thermometer), resistive heater, pressure sensor (placed on top of a dedicated membrane) and finally on the window membrane there will be electrodes for electrochemistry in addition to structures that will help reduce charging of the system when under electron irradiation.. Keeping things simple is a general design philosophy, and it has therefore been chosen to make all these sub-devices in one layer. This report only describes the use of gold, but it would obviously be interesting to try other metals, and maybe ultimately produce the different sub-devices in different materials.

2.2 The membrane

The key element of the device is the very thin nitride membrane usable for electron microscopy. Prior to our work, experiments had been carried out using a 100 nm thick membrane, but since the resolution is dependent on the membrane thickness, it would be interesting, via simulations and later experiments, to determine whether it is possible to make and use even thinner membranes. Here the important questions are how well the membrane can withstand the pressure difference between cell and chamber, and if it is damaged from general handling. An answer to the first part can be given based on simulations, while it must be up to experience from use to answer the last one. It should also be noted that the requirement could be different for different experiments, if one just wants to keep a liquid inside the cell, then the pressure difference will only be 1 bar. It would however also be interesting to carry out chemical reactions that would create a higher pressure, and for this a thicker membrane might be needed. For a system with flow, a pressure could also build up locally at the membrane, which would require a certain durability.
The role of the membrane is first of all to be the window used to 'look through', in this design featuring electrodes for electrochemistry. Furthermore, the pressure sensor will utilize the membrane deflection, to induce a resistance change in a strain defendant resistor placed on top of it.
In this chapter, we will look at general theory of membranes and lay out some simple simulations that will give an idea about what the deflection looks like and what kind of pressures the membrane can withstand.

2.2.1 Silicon nitride

The material of choice for the membrane is silicon nitride, Si_3N_4, which is commonly used as a diffusion barrier in MEMS-technology. Because of its high elastic modulus, brittless (elastic up until point of fracture), and high fracture strength, it is also a very good choice for membranes [Kovács et al., 2007]. The mechanical properties are highly defendant on the way the nitride is grown, but for the next calculations, experimental values are taken from [Edwards et al., 2004] and are 255±5 GPa, 5.87±0.62 GPa and 0.23±0.02 for Young's modulus, fracture strength and Poisson's ratio respectively.
The nitride used for these membranes is grown with a special silicon rich recipe giving a very low stress, and for free-standing membranes this is obviously very important. Stoichiometrically grown nitride has a built-in compressive stress, that would deform the membrane as soon as the silicon support was gone, there would be too much material so too speak. Contrary to this, the low-stress nitride possesses a slight tensile stress, that will give a nice flat membrane once etched out.

2.2.2 Heavy p-type doping as etch stop

During the design phase, the option of supporting the membrane with a grid of heavy p doped silicon was discussed. It is known that p+ doping with boron can act as an etch stop in KOH [Collins, 1997], and in this case, it could be used to maintain a grid of thick rigid silicon under the membrane. The big problem about this technique is though, that heavy boron doping induces a lot of stress in the silicon because of the big difference in atomic radius of the two elements. For this reason, and to cut down on process steps, it was decided to make a design with unsupported membranes.

2.2.3 A first look at membranes, small deflection

A starting point for looking at membranes was Roark's Formulas for Stress and Strain [Young and Budynas, 2002] that gives easy to use formulas for stress and deflection of bending plates. The formulas apply when: "'*(1) The plate is flat, of uniform thickness, and of homogeneous isotropic material; (2) the thickness is not more than about one quarter of the least transverse dimension, and the maximum deflection is not more than about one-half the thickness; (3) all forces—loads and reactions—are normal to the plane of the plate; and (4) the plate is nowhere stressed beyond the elastic limit*
The first condition is fulfilled, for (2), the first part is true, while it is unsure whether the second one is, (3) should be ok and (4) is also unknown at this point. The formula for maximum deflection y_{max} of a rectangular plate of width b, length a and thickness t with all edges fixed under uniform pressure q is given as:

$$y_{max} = \frac{\alpha q b^4}{E t^3} \tag{2.2.1}$$

where the value of α is found in a table and is function of the ratio between a and b. E is the Young's modulus of the material. The formula does not take Poisson's ratio into account, but it is stated that the error should be no larger than 8% for Poisson's ratio between 0.15 and 0.30. If we take a membrane of dimensions $50{\times}300\mu\text{m}^2$ α is 0.0284 and put on a loading of 1 bar = 100kPa, it gives $y_{max} = 5.68 \cdot 10^{-4}$m or 568$\mu$m. This deflection is huge and it does not seem likely that it is correct. We were rather puzzeled by this result at first, but obviously, when looking at the conditions for the formula, one must realize that the deflection of a very thin membrane like this one is (much) larger than half the thickness, and the linear formula no longer applies.

2.2.4 Large deflection, a closer look at theory of thin membranes

What separates a small deflection from a large on, is the fact, that as the deflection becomes larger, a tensile stress is build up in the middle section of the membrane. This makes it stiffer and thus results in less deflection for a giving load level[Young and Budynas, 2002].

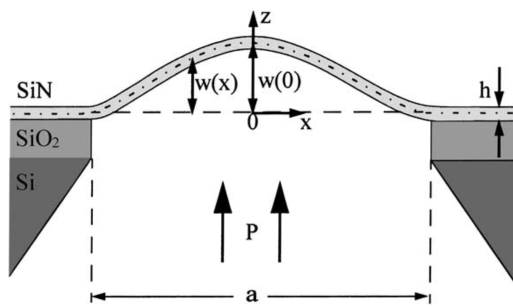

Figure 2.2: Membrane of width a deflected under pressure P, profile according to function $w(x)$. Neutral fiber marked with dashed line. (property of [Yang and Paul, 2002])

[Yang and Paul, 2002] presents a model for the deflection of a thin membrane that will be applied here. For greater detail and full listing of equations, turn to Appendix 1.
The system under study is a thin membrane loaded with a uniform pressure P as seen on figure 2.2. The membrane deflection profile is described by the function $w(s, x)$ where x is the coordinate across the membrane, with $x = 0$ in the center, and s denotes the in-plane stress in what is referred to as the 'neutral-fiber'. This fiber is the middle of the membrane (dashed line in figure 2.2), and here the stress is approximately independent of x coordinate.

All variables are transformed into reduced dimensionless variables denoted with a "$^-$"
The model will now be applied to calculate the center (maximum) deflection of the membrane described in section 2.2.3 under 1 bar pressure and with no pre-stress.

The problem is non-linear in nature, the deflection profile depends on the in-plane stress, while the in-plane stress on the other hand depends on the deflection. The equations are then solved in the following way:
The center deflection $\bar{w}(\bar{s}, 0)$ is given by:

$$w_0 = \bar{w}_0(\bar{s}, 0) = \bar{P}G(\bar{s}, 0) \tag{2.2.2}$$

and the in-plane stress

$$\bar{s} \ = \ \bar{s}_0 + \frac{1}{2} \cdot \bar{w}_0^2 \cdot H(\bar{s}) \tag{2.2.3}$$

The transcendental functions $G(\bar{s}, \bar{x})$ and $H(\bar{s})$ are listed in Appendix 1. Equation 2.2.2 is now inserted into equation 2.2.3 yielding

$$\bar{s} \ = \ \bar{s}_0 + \frac{1}{2} \cdot (\bar{P}G(\bar{s}, 0))^2 \cdot H(\bar{s}) \tag{2.2.4}$$

only variable is $\bar{s}$ and that allows for a numerical solving which gives $\bar{s} = 1777.73$ and transformed it gives $s = 0.469GPa$. By insertion into equation 2.2.2 one get $w_0 = 1.30\mu$m
The model presented here is a much more correct analytical approach to the problem of deflection of a very thin membrane, and the result does indeed seem a lot more reasonable. The model will also prove its worth later, when it is used to give estimates for the Young's modulus and build-in stress based on actual measurements of deflection.

2.2.5 Membrane fracture

For reasons mentioned, the fracture pressure of the membrane is of great interest. The in-plane stress is roughly homogeneous throughout most of the membrane, except around the edges. Here, a very large stress is built up, and a fracture is likely to occur at the edges. [Yang and Paul, 2002]
The maximum stress s_{max} is also described by the model and given by

$$s_{max} = s_{fr} + \frac{1}{2} h E_{ps} w''(s_{fr}, \pm a/2) \tag{2.2.5}$$

where w'' denotes two times differentiation with respect to x
In the discussion of membrane fracture and possible thicknesses of membranes, we will rely on simulations rather that this approach.

2.3 Simulations of membrane deflection

When we first started out with the simulations, we were very keen on doing big 3D simulations of the system. It would turn out though, that it is not such a trivial thing for the system studied here. For the simulations, creating a good mesh is of very great importance, something that is not easy to do when the ratio between the dimensions of the system is very large, i.e. the structure is very thin. Figure 2.3 shows the deflection of a $50 \times 300 \mu\text{m}^2$ membrane. It should be noted, that when we first started out using Comsol on these systems, we where again very puzzled by the huge deflections it gave, something like 15μm for a 1 bar pressure difference. It turned out then, that the stress-strain package had an option called "‘large deformations"’ that had to be enabled. Much similar to our analytical approach, this changes the equations from being linear to being non-linear, and

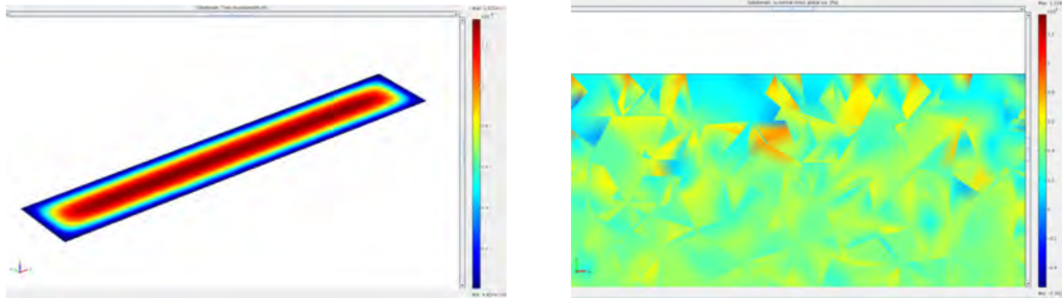

Figure 2.3: View of a 3D model of the membrane, plot showing deflection

Figure 2.4: Stress in the y-direction, mesh is clearly not optimal

the response seemed much more reasonable.
Figure 2.4 demonstrates the problem of creating a good 3D mesh. The mesh used was quite fine (small elements), but on the edges of the membrane, still not nearly good enough. As can be seen on the figure, that shows stress in the transverse direction, the stress level varies a lot from element to element and this is "‘not a good simulation"’. Later in the project, we have turned to modeling in 2D, which is far superior, and in the next section we will take a look at that.

2.3.1 2D model

In 2D it is possible to model the cross-section of the membrane using the package 'plane strain' which is exactly intended for a cross-section of a very long system. Here, one membrane is 50 by 300 microns and the other is 50 by 900, so the membrane can be regarded infinitely long and modeled in 2D.
The first steps of the simulation is to define the geometry, boundary conditions and physics. The membrane under study is again 50 microns wide and 50 nm thick, and the modeled geometry is a rectangular cross-section of these dimensions. To fully model the interface between membrane and the surrounding nitride, a 10 micron by 50 nm rectangle is placed on both sides of the membrane. The lower boundaries of these surrounding domains are fixed and the rest of the boundaries are free. On the lower boundary of the membrane a load of -100 kPa or -1 bar is applied. Comsol has a build in material library, where Silicon Nitride has Young's modulus 250 GPa and Poisson's ratio 0.23 It has been chosen to set the Young's modulus to 255 GPa as discussed earlier.

2.3.2 Meshing

Making a good mesh is a trade off between calculation speed on one side and accuracy on the other. Luckily Comsol 3.5 is equipped with a feature called adaptive meshing, that will solve the problem, then recalculate the mesh making it denser where it is needed, and solve the problem again. This version of Comsol was released during the course of the project. In figure 2.5 the initial mesh is seen in the area around the boundary of the membrane (right side). This mesh consists of 4042 elements and is created with the free mesh creator. As can be seen, this mesh is actually pretty coarse in the y-direction, but because of the huge length to thickness ratio of the system, the number of elements is quite high. Using the adaptive meshing two times changes the mesh to that displayed in figure 2.6, now consisting of 21806 elements. As can be seen, the mesh is only changed in a narrow interval of around 3 μm around the boundary, but to a very dense mesh. This clearly displays what was also seen earlier; in most of the membrane there is only in-plane

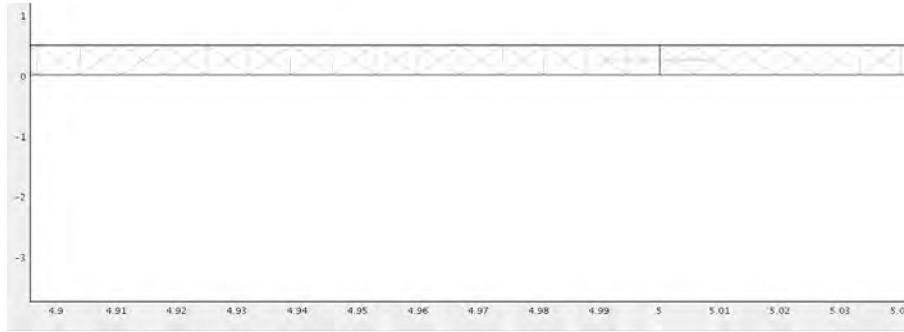

Figure 2.5: Mesh before adaption, 2D model of membrane

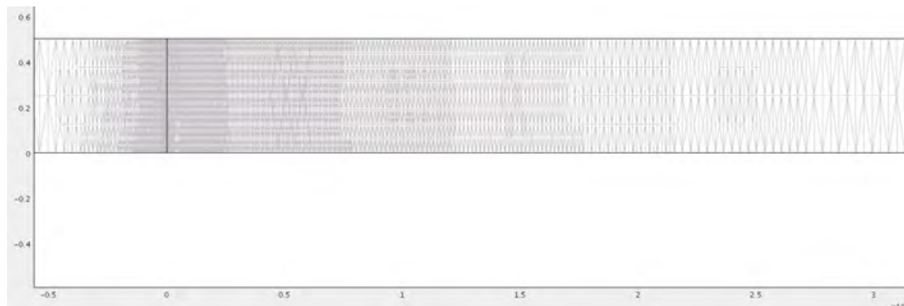

Figure 2.6: Mesh after 2 adaption steps, very very dense in the edge region, but quickly changes back to the original mesh in most of the structure (N.B axis not even)

stress, homogeneously distributed throughout the thickness of the membrane. Close to the edges however, the stress-gradient through the membrane is huge and a very dense mesh is required in order to model it correctly.

2.3.3 Postprocessing

After having solved the problem, there are various options for postprocessing. First and foremost, it is possible to plot different parameters. In figure 2.7 a close-up plot of the stress in the x-direction very close to the bottom of the edge is shown. It is seen, that there is a huge compressive stress here, -14 GPa, in the lowest 0.5 nanometers of the structure. The blue triangle resembles a mesh element, and by no coincidence. It shows a problem or effect in finite element simulations, that one has to be aware of; singular points will arise and they belong to the simulation and are not physical. When plotting, it is possible to manually specify the lower limit, and in figure 2.8 a larger section of the membrane is shown, now with a more useful scale. A further refinement of the mesh would smoothen out this 'compressed singularity' but it would still be there.

2.3.4 Results

A simulation of the membrane at 1 bar pressure gives a displacement $w_0 = 1.29\mu$m. The in-plane stress is seen in figures 2.9 and 2.10 and ranges from 440 MPa to 500 MPa, around 472 MPa in the neutral fiber. These results are in very good agreement with the results from the large deflection model that gave a neutral fiber stress of $s = 0.469GPa$ and a center deflection of $w_0 = 1.30\mu$m

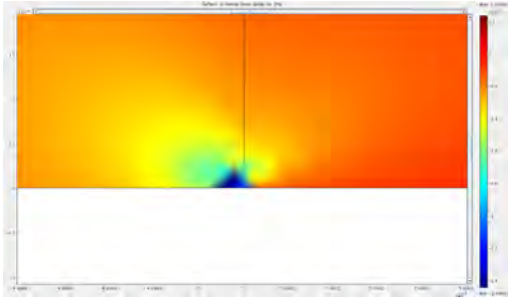

Figure 2.7: Huge compressible stress in one or a few mesh elements at membrane edge. 1 bar pressure.

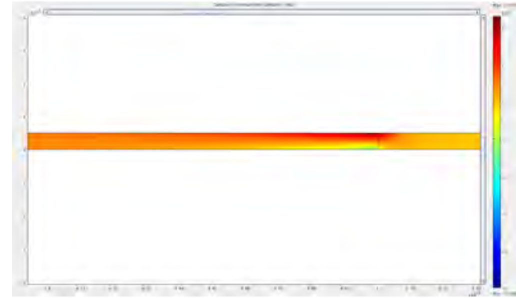

Figure 2.8: High or unphysical stress cut away from the scale to give a more useful plot

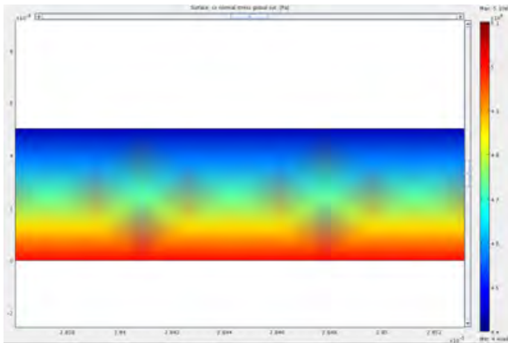

Figure 2.9

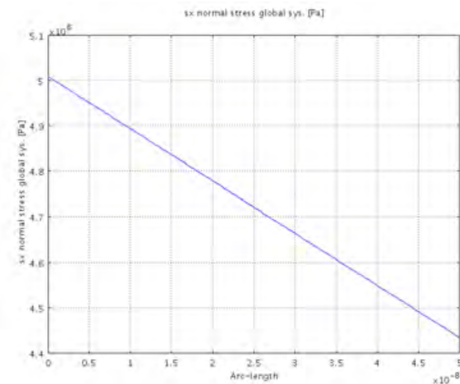

Figure 2.10

Membrane strength, fracture

As mentioned, [Edwards et al., 2004] reports the fracture strength of silicon nitride to be 6.87 GPa. This number could be different for the nitride used here, but will be used as a guideline in the design process of the membranes. In figure 2.11 the stress profile is seen around the edge for the 50 nm thick membrane.

Table 2.1: Fracture pressures for different membrane thicknesses (assuming fracture stress is 6.87 GPa) Modeling thinner structures than 40 nm is quite troublesome and has not been done

Thickness [nm]	Pressure [bar]	Tensile stress [GPa]
40	4.4	6.81
50	5.5	6.81
75	8.3	6.82
100	11.2	6.86

Based on the simulations shown in table 2.1 it was decided to first produce a batch of wafers with 50 nm nitride and run the process on those. It was the original plan to try other thicknesses as well, but it was not realized within the time of the project. As can be seen, a 50 nm membrane should withstand up to 5.5 bar pressure, but since the exact fracture strength and stability of the membranes during processing, dicing and general handling of the chip, was unknown in the design phase, it was decided to go with this pretty big safety margin (with respect to the 1 bar pressure difference inside the SEM). It should also be mentioned, that the experiments carried out at Nanotech prior to our work was on 100 nm membranes, so going to 50 nm would already mean a huge improvement. Based on the

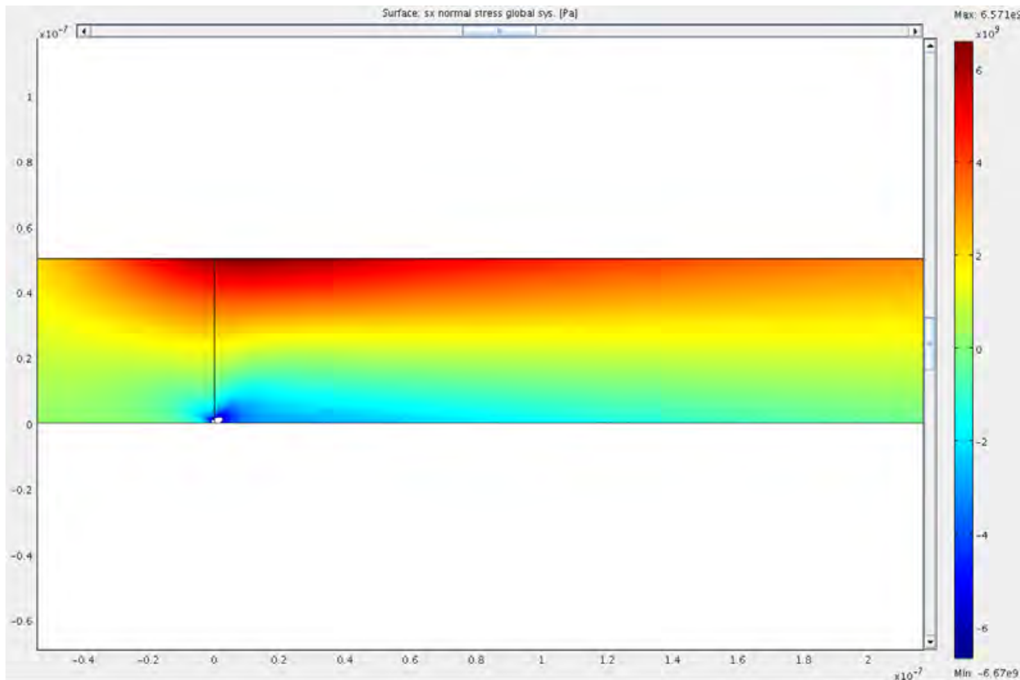

Figure 2.11: 50 nm membrane under 6.2 bar pressure, tensile stress in edge region is 6.57 GPa, almost the fracture stress reported by [Edwards et al., 2004]

experience with the 100 nm membranes, they were breaking quite easily, there was even some uncertainty whether or not working with 50 nm membranes would be possible. As will be shown, this was indeed possible.

2.4 Pressure sensor

The idea and working principle behind the pressure sensor is to place a strain gauge on top of a membrane. When the membrane deflects, it will induce a resistance change in the gauge, which can be measured.
In the design phase, it was the intention to figure out if this would even be possible, would the changes in resistance be measurable? Gold will be the focus material in the simulations, but other materials with higher response could obviously also be interesting to use.

2.4.1 Piezoresistivity

Piezoresistivity means that a materials resistance changes as function of mechanical stress. There are two contributions to this, firstly a geometrical change; a strained piece of conductor will change its dimensions according to mechanical properties, and with that follows a change in resistance. Secondly, the resistivity itself will change, a strained lattice will result in a change in resistivity. For a slab of material, the relative change in resistivity $\Delta R/R$ as function of strain in the length direction ϵ_L is expressed as [Thomsen and Richter, 2007]:

$$\frac{\Delta R}{R} = (1+2\nu)\cdot\epsilon_L + E\pi_L\epsilon_L \tag{2.4.1}$$

$$= \gamma\epsilon_L \tag{2.4.2}$$

where ν is Poisson's ration, E is young's modulus, π_L is the piezo coefficient in the length direction and finally γ is called the gauge factor.
The change in resistivity is a lot more pronounced in semiconductors than in metals, π_L is high, because a strain will change the band gap, and thereby the number of electrons in the conduction band. For semiconductors this response is often strong enough to allow for neglection of the geometrical term . With respect to piezoresistivity, this makes semiconductors an excellent strain gauge.
Metals on the other hand experience very little change in resisitivity, and here the geometrical term will be dominant, and the response generally much smaller. How dominant, does not seem to be completely agreed on though, and different suggestions can be found in litterature. In [Thomsen and Richter, 2007] it is stated that π_L can be completely ignored which means that $\gamma = (1+2\nu)$, this simplification is probably due to the fact that the note is used in a course teaching how to make a semiconductor pressure sensor.
According to [Parker and Krinsky, 1963] the gauge factor for gold and platinum is:

$$\gamma = 2(1+\nu) + 2G(1-2\nu) \tag{2.4.3}$$

where G is the Grüneisen parameter. The change in resistivity

$$d\rho/\rho/\epsilon_L = 1 + 2G(1-2\nu) \tag{2.4.4}$$

is accounted for by changes in the phonon amplitudes in the stressed crystal, leading to a change in electron-scattering probability. The Grüneisen parameter is generally between 2 and 3 for metals [Parker and Krinsky, 1963], and will not be calculated here. According to [Jen et al., 2003] values for thin films lies at $\gamma = 1+3\nu$ which is lower than the bulk value, for films thicker than the electron mean free path (conductance in thin films will be mentioned in a later chapter). For films much thinner than the mean free path, the gauge factor is known to increase sharply. Making such thin films is not an option in this case, since the metal layer has to be used for the other sub-devices. For the calculations in the next sections, γ is set to the thin film value $1+3\nu$ which gives $\gamma = 2.32$ for gold.

2.4.2 Temperature response

Using strain-induced resistance changes in metal for pressure measurements is not without problems. Temperature changes will also affect the resistance of the strain gauges, both in terms of resistivity change as function of temperature, but also mismatch in thermal expansion coefficient of the metal and substrate can give strain induced resistance changes. In a perfect world, these effects should be removed by the way the gauges are connected, as shall be seen in next section, but most likely temperature will play a role.

2.4.3 Proposed design

During the design phase, several different approaches was considered, something that will not be further discussed here. It was decided to work with a design, of which a section can be seen in figure 2.12a. Here, 20 μm long wires are placed with 15 μm on the membrane. They are 5 μm wide, placed with 5 μm spacing (so pitch is 10 μm) and connected with 5 μm wide wires. As shall be seen, simulations clearly show the highest strain to be at the edges, and this design utilizes that. In this way, two strain gauges are placed on a dedicated membrane, image of the actual chip can be seen in figure 2.12c

2.4.4 Wheatstone bridge

To measure the resistance changes in the two strain gauges, they are placed in a Wheatstone bridge, which allows for measurement of very small resistance changes. It consists of 4 resistors and the schematic layout can be seen in figure 2.12b. A voltage V_S is supplied to the bridge and the voltage V_0 can be measured. The expression linking these voltages with the resistances is given as[Thomsen and Richter, 2007]:

$$V_{out} = \left(\frac{R_4}{R_3 + R_4} - \frac{R_2}{R_1 + R_2} \right) V_S = \frac{R_1 R_4 - R_2 R_3}{(R_1 + R_2)(R_3 + R_4)} V_s \tag{2.4.5}$$

First of all, it can be deduced that the resistors placed on the membrane (the strain gauges) must be connected as R_1 and R_4. There must be a similar change in resistance for these two, it should increase, which again should give an increase in V_S. If R_2 and R_3 could decrease when R_1 and R_4 increase, this could give an even stronger response, something that is realized in semiconductor MEMS pressure sensors. In this design however, this is not possible, but still the resistors R_2 and R_3 play a role in the setup. The point is, that temperature changes, as mentioned, will affect the resistances, but if the bridge is perfectly symmetrical, that is $R_1 = R_2 = R_3 = R_4$ at $P = 0$ bar, the changes as function of temperature should be the same for all resistors and V_{out} should not be affected.
Assuming that the changes in R_1 and R_4 is the same, and this change is $\delta \cdot R$, $\delta = \Delta R/R$, all resistances will be:

$$R_1 = R(1 + \delta) \tag{2.4.6}$$
$$R_2 = R \tag{2.4.7}$$
$$R_3 = R \tag{2.4.8}$$
$$R_4 = R(1 + \delta) \tag{2.4.9}$$

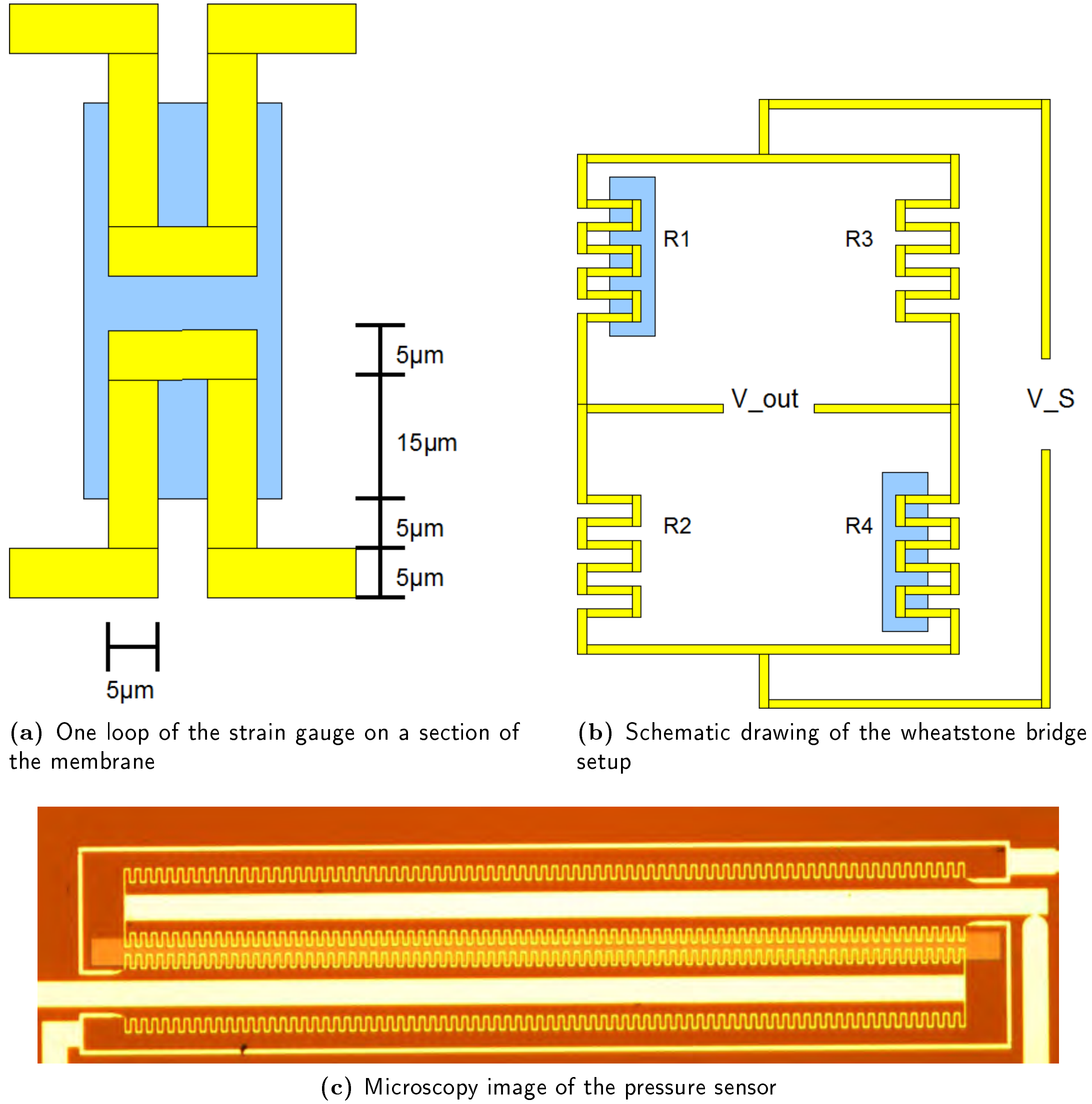

(a) One loop of the strain gauge on a section of the membrane

(b) Schematic drawing of the wheatstone bridge setup

(c) Microscopy image of the pressure sensor

Figure 2.12: The pressure sensor layout

and equation 2.4.5 can be rewritten:

$$V_{out} = \frac{R(1+\delta)R(1+\delta) - R^2}{(R(1+\delta)+R)(R+R(1+\delta))}V_s \quad (2.4.10)$$

$$= \frac{R^2(1+\delta)^2 - R^2}{(R(1+\delta)+R)^2}V_s \quad (2.4.11)$$

$$= \frac{R^2(1+\delta^2+2\delta) - R^2}{4R^2+4R^2\delta+R^2\delta^2}V_s \quad (2.4.12)$$

$$= \frac{\delta^2+2\delta}{4(1+\delta)+\delta^2}V_s \quad (2.4.13)$$

$$= \frac{\delta^2+2\delta}{(2+\delta)^2}V_s \quad (2.4.14)$$

With equation equation 2.4.14 and with the relationship $\Delta R/R = 2.32 \cdot \epsilon_L$ for gold, it should now be possible to predict the response of the pressure sensor, if the strain in the gold can be modeled, which will be done in the next section.

2.4.5 Simulations of response

The modeling is just as described in section 2.3, with the geometry as illustrated on figure 2.13. In this case though, the parameter of interest will be mainly the strain, instead of stress.

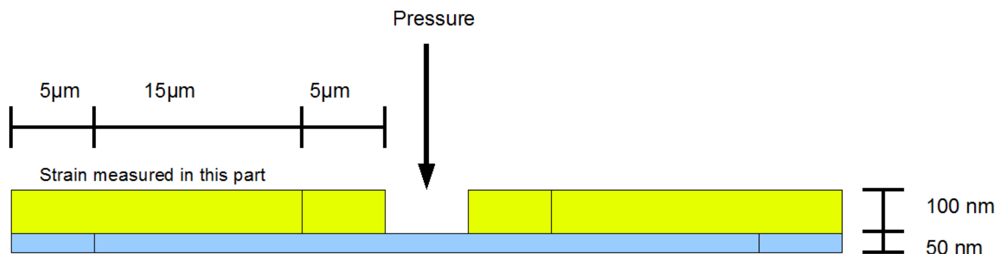

Figure 2.13: 2D geometry as modeled in Comsol. The gray part is nitride and the yellow illustrates gold.

Simulating strain

Figure 2.14 is an example of the strain profile as simulated by Comsol. Notice how there is a very narrow region with a high strain just around the edge, and then a more homogeneous profile through the rest of the membrane. For now, the response of the sample will

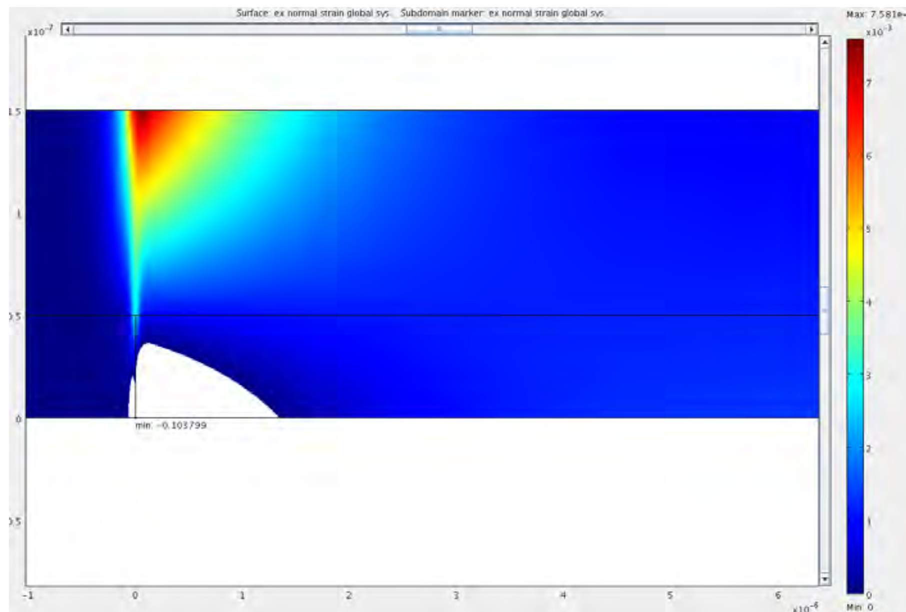

Figure 2.14: Strain profile, 1 bar. All negative strain removed from plot (white area) Notice how the strain is high in a very narrow region $\tilde{1}\mu$m, then lower and homogeneous at the rest of the membrane. Left side is not on the membrane and therefore darker (zero strain) N.B axis are not even

be approximated by a mean strain in the length direction ϵ_L
In Comsol, the function boundary integration is used to sum up the strain in the strain gauge wire (see figure 2.13). This quantity is given as an area, and then dividing this number by the original area of the wire will give the mean strain throughout the structure. The 2D cross section of the wire is 100 nm by 20 μm giving a total area of $2.0 \cdot 10^{-10}\text{m}^2$ At 1 bar, the integrated strain, or 'added cross section area' has the value $1.93 \cdot 10^{-15}$ which

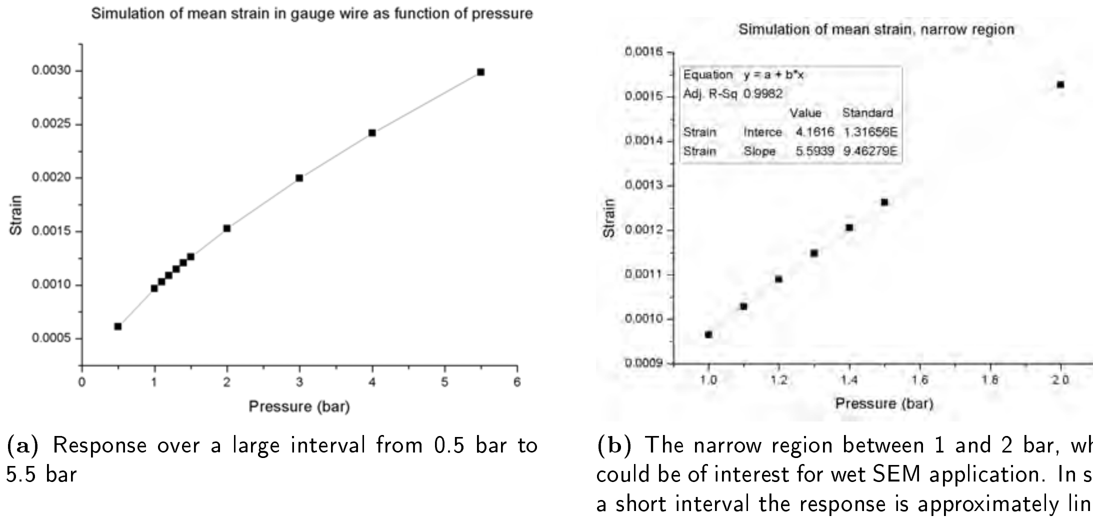

(a) Response over a large interval from 0.5 bar to 5.5 bar

(b) The narrow region between 1 and 2 bar, which could be of interest for wet SEM application. In such a short interval the response is approximately linear.

Figure 2.15: Comsol simulation of mean strain in the 100 nm thick and 20 μm long strain gauge wire at different pressures.

again gives a mean strain $\epsilon_L = 9.67 \cdot 10^{-4}$ or 0.0967%
To give an idea about how the pressure sensor will respond to pressure, the first thing to consider is the value of the mean strain for different pressures. In figure 2.15 mean strain is plotted versus pressure as simulated in Comsol. The relationship is not linear, but as it is seen from the figure, in a small interval, it comes quite close, which will also be seen later from the actual measurements on the pressure sensor.

Response of the Wheatstone bridge

In the design phase, the main purpose of what is described in these sections, was to establish an idea of the feasibility in a pressure sensor design like this. In this section, it will be shown what kind of response the Wheatstone bridge can be predicted to give.
To do that, the bridge is divided into unit cells like on figure 2.16, that shows a Comsol simulation of the resistance in the structure. A potential difference of 1 V is set at the boundaries and then the current through the structure is displayed, and the resistance is the found through Ohm's law.

$$R = \frac{U}{I} \tag{2.4.15}$$

This is $R_{cell} = 1.34\Omega$ for the entire cell and $R_{strained} = 0.877\Omega$ for the strained part alone, witch is assumed only to be the part of the wire perpendicular to the membrane edge. This assumption also leads to $\Delta R_{cell} = \Delta R_{strained}$.
The reason that these number are needed is that the δ to be used for equation 2.4.14 must be the relative resistance change of the entire unit cell rather than just for the strained wire. If the simulated mean strain is called ϵ_{mean}, the relative resistance change δ, the gauge factor γ and the resistances as above, then:

$$\delta = \frac{\Delta R_{cell}}{R_{cell}} \wedge \frac{\Delta R_{strained}}{R_{strained}} = \gamma \epsilon_{mean} \tag{2.4.16}$$

$$\Downarrow \tag{2.4.17}$$

$$\delta = \frac{\gamma R_{strained}}{R_{cell}} \epsilon_{mean} \tag{2.4.18}$$

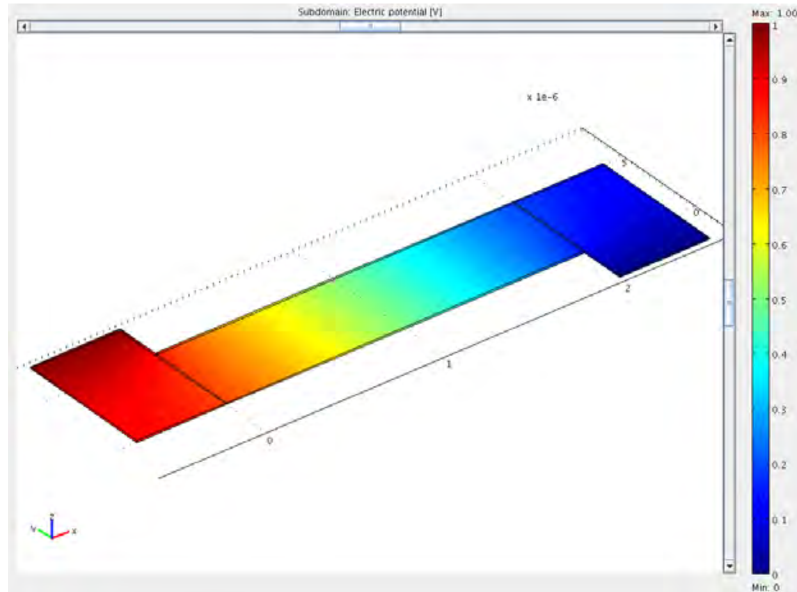

Figure 2.16: Strain gauge unit cell. Simulation shows potential.
Resistance of entire cell is 1.34Ω and of strained wire it is 0.87Ω

with $\gamma = 2.32$ it gives

$$\delta = 1.518 \cdot \epsilon_{mean} \tag{2.4.19}$$

The values related to the simulated strains is presented here in table2.2. If this is correct,

Table 2.2: Predicted response for the strain gauge

Pressure [bar]	Strain	V_out[mV] (for $V_s = 1.5V$
0.5	$0.612 \cdot 10^{-3}$	0.696mV
1.0	$0.966 \cdot 10^{-3}$	1.10mV
1.1	$1.028 \cdot 10^{-3}$	1.17mV
1.2	$1.089 \cdot 10^{-3}$	1.24mV
1.3	$1.115 \cdot 10^{-3}$	1.31mV
1.4	$1.121 \cdot 10^{-3}$	1.37mV
1.5	$1.262 \cdot 10^{-3}$	1.44mV
2.0	$1.527 \cdot 10^{-3}$	1.74mV
3.0	$1.998 \cdot 10^{-3}$	2.27mV
4.0	$2.418 \cdot 10^{-3}$	2.75mV
5.5	$2.987 \cdot 10^{-3}$	3.39mV

the pressure sensor should give a response of around 0.06 mV per 0.1 bar pressure change, which should be possible to measure. Based on this, the requirement of 0.1 bar sensitivity should be achievable.

2.5 Thermistor

After consulting an expert in the area here at Nanotech, it was learned that a thermistor was usually designed to have a resistance R_0 between 2 and 7 kΩ, so this would also be the value this design should aim for.
The resistivity, ρ, of bulk gold is $\rho_0 = 2.051 \cdot 10^{-8}\Omega$m at 20°C ([CRC, 2008]). If the thickness t of the gold is 100nm and the wanted resistance at room temperature is to be between, R_0=2kΩ and R_0=7kΩ, the thermistor (assumed to be a single long wire) length to width ratio, L/w given by

$$R_0 = \rho_0 \frac{L}{tw} \quad (2.5.1)$$

$$\frac{L}{w} = \frac{R_0 t}{\rho_0} \quad (2.5.2)$$

should be between

$$R_0 = 2k\Omega \Rightarrow \frac{L}{w} = 9751 \quad (2.5.3)$$

$$R_0 = 7k\Omega \Rightarrow \frac{L}{w} = 34130 \quad (2.5.4)$$

In operating temperature range, resistivity for metals is assumed to depend linearly on temperature, and the resistance as function of T is given by:

$$R(T) = R_0(1 + \alpha(T - T_0)) = R_0(1 - \alpha T_0) + \alpha R_0 T \quad (2.5.5)$$

Where α is the temperature coefficient of electrical resistance at T_0 and R_0 is the resistance at T_0
For $T_0 = 20^o$C, α is reported to have the value 0.0034K^{-1} [wik]. This gives a temperature dependency of

$$R(T) = 0.9286 \cdot R_0 + 0.0034\text{K}^-1 \cdot R_0 \cdot T \quad (2.5.6)$$

and

$$R_0 = 2k\Omega \Rightarrow R(T) = 1857.2 + 6.8^0\text{C}^{-1} cdot T \quad (2.5.7)$$

$$R_0 = 7k\Omega \Rightarrow R(T) = 6500.2 + 23.8^0\text{C}^{-1} cdot T \quad (2.5.8)$$

$$(2.5.9)$$

Both of these slopes (6.8Ω^0C^{-1} and 23.8^{0}C^{-1}) should be easy to detect, and designing the thermistor with 9751<$\frac{L}{w}$<34130 seems absolutely reasonable. If decided that the width of the wire in the thermistor is to be 5μm the required length will then be between, 4.88cm<L<17.06cm.

2.5.1 Mask design of thermistor

For a picture of the thermistor, see figure 2.18c or a close-up in figure 3.10 To achieve these requirements the thermistor was constructed of 60 parallel 1295μm long straight wires with 5 μm spacing. These where connected at the ends with 59 wires, 15μm long and also 5μm wide. To calculate the resistance, these are divided into 59 5×5μm^2 wires and 118 5×5μm^2 corners, since the resistance through the corners is approximately half

that of an equivalent square. This again means that the thermistor design is equivalent of a $60 \cdot 1295\mu$m$+2 \cdot 59 \cdot 5\mu$m= 7.8cm straith wire
This gives a total resistance of R_0=3.445kΩ.
This R_0 lies within the desired range, and thus enables use of the design with thinner or thicker films than the 100nm, without destroying the sensitivity.

2.6 Heater

To heat up the chip, a resistive heater has to be placed on the chip, and it will, as the other sub-devices, be made of gold. The strategy for heating will be to heat up the entire chip, contrary to heating locally on the membrane.
To give an idea of the range in which the power output of the heater needs to be, a 'quick and dirty' blackbody model is used. Here, the chip is assumed to be a black body of a temperature T emitting radiation with a power P according to the Stefan-Boltzmann law:

$$P = \sigma A T^4 \tag{2.6.1}$$

where σ is the Stefan-Boltzmann constant, A is the total surface area of the chip and T is the (absolute) surface temperature. σ=5.67004$\cdot 10^{-8}$ W$\cdot$m^{-2}K^{-4} and $A = 2 \times 8.5 \times 12\mu$m^2
If P is the power supplied to the chip by the heater, then T will be the temperature in the steady state. If a steady-state temperature of 100°C is desired, P has to be 0.22W. Since this is only taking into account radiation from chip and not from the entire sample holder, the design will aim for a power of 0.5W. These calculations are done in order to make it possible to control the heating directly with a Labjack DAQ that has a maximum voltage of 5V. For this reason the resistance has to be tuned correctly in order to reach the desired power output of 0.5W
The design of the heater is shown in figure 2.17, it has a length of 3.82cm and is 200μm wide. If, as in the thermistor, the thickness of the gold is 100nm this gives a resistance in the heater, R_0=46.6Ω, which will give a power of P$\approx$0.5W if connected to a 5V source. Should this power be insufficient in reaching a desired temperature, it is of course always possible to heat with a higher voltage.

2.7 ZIF-connection

The chip is designed to fit into a so-called ZIF socket for electrical connection, and thus does not rely on wire bonding. The ZIF-socket can be seen in figure 2.18a. The downside is that the chip has to be quite big, so this approach will not be possible in a future TEM version of the device. For this project though, the added flexibility in terms of packaging and quick and easy management of connections, makes this approach absolutely perfect.
The chip will need 14 connections, therefore a 16 pin ZIF socket is chosen. The selected model has number '52892-1690' at RS-components, and has an internal width of 8.5mm. The chip then needs to have this width and the area of connection electrodes must be at least 3.5mm long. The pitch size of the pins is 500μm.
The ZIF connection electrodes on the chip is shown on figure 2.17, notice how the electrodes are not reaching the bottom of the chip, but instead a small area of clean nitride is left to prevent the risk of Si-metal interfaces, which might lead to short-circuiting.
The chip shown in figure 2.17 has been used, so (apart from it being dirty) it is possible to see exactly where the connection to the ZIF-socket has been made, the small dots on the electrodes are where the socket has locked in.

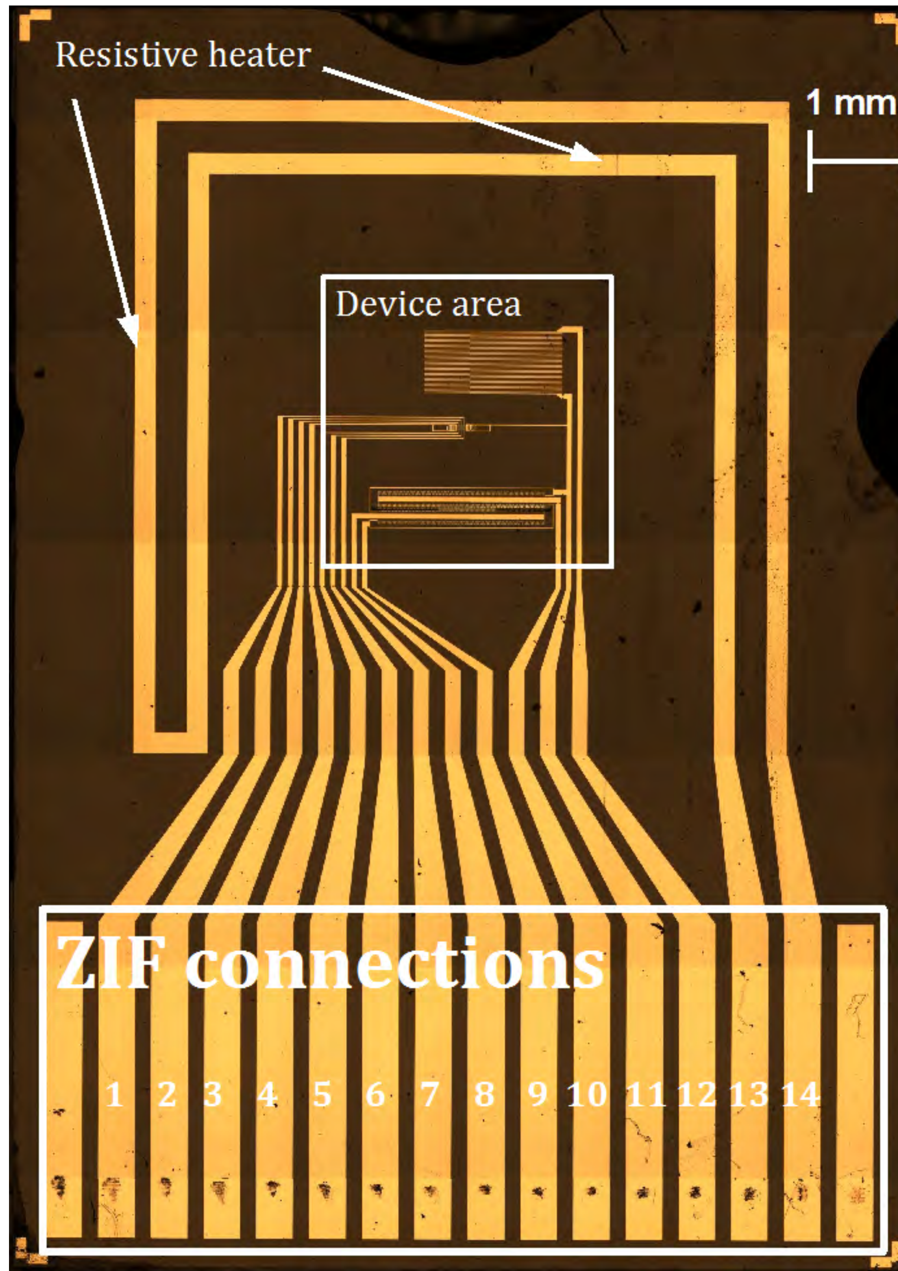

Figure 2.17: Microscopy image of the entire chip

2.8 Final layout

After all initial considerations, a design was made using the software 'L-edit' and transferred to a mask to be used for the fabrication of the device. Pictures of the final chip is seen in figures 2.17 and 2.18c.
The main idea is that the three important sub-devices; pressure sensor, thermistor and window, are place in a $3\times3\mu\text{m}^2$ square, but the chip is made to fit a ZIF socket. The heating is done by heating the entire chip using a resistive heater placed close to the edge.

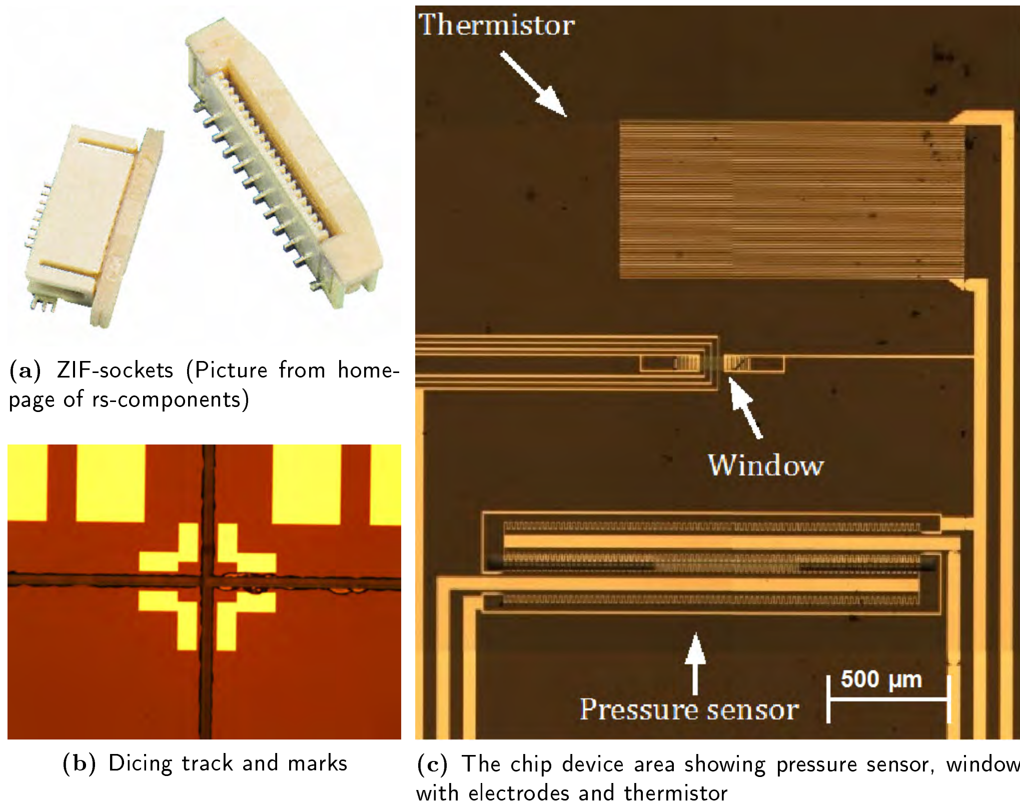

(a) ZIF-sockets (Picture from homepage of rs-components)

(b) Dicing track and marks

(c) The chip device area showing pressure sensor, window with electrodes and thermistor

(d) Window area with electrodes

Figure 2.18

2.8.1 Window

The window is 50 × 300 μm^2 and on it is placed 6 electrodes, with gaps 3, 6 and 9 μm as can be seen from figure 2.18d These are to be used as electrodes for electro chemistry and narrowing of the gaps using electroplating. Here it is important, that the electrodes nowhere on the device are placed closer that the size of the electrode gaps, since the plating will take place on the entire electrode.
Furthermore, two structures are also placed on the membrane, and the idea here is that they can be used for discharging during electron microscopy, whether this will work or not will be up to experiments to tell.

2.8.2 Dicing marks

Dicing marks are made in the corners of the chips to allow for correct sawing. Such a mark is seen in figure 2.18b together with the track made from the dicer.

2.8.3 Electrical connections

Here follows a listing of all electrodes and what they refer to on the chip. Numbering is from left to right, as the chip is viewed in figure 2.17

Table 2.3: Chip electrical connections as seen in figure 2.17

#	Name
1	Electrode 3a
2	Electrode 2a
3	Electrode 1a
4	Discharger
5	Electrode 1b
6	Electrode 2b
7	Electrode 3b
8	$V_{out}1$
9	V_S1
10	$V_{out}2$
11	Common ground
12	Thermistor2
13	Heater1
14	Heater2

3

Fabrication

3.1 Process

In this section, all processes done in the cleanroom to produce the device will be shortly introduced. A process flow chart is attached in Appendix 3, the numbers mentioned in this section, i.e. (2.1), refer to that chart.
In short the process is as follows: First a nitride is grown, then this nitride is used as mask for KOH etching and at the same time it will form membranes on the front side. After this and a second lithography step, metal is deposited on the wafer front side and the chips are ready to be diced (sawed out).

Nitride membrane (step 1.2)

The first thing to do is to grow a low stress Silicon nitride membrane in the LPCVD (Low Pressure Chemical Vapor Deposition) oven. The LPCVD is done in a oven where NH_3 (ammonia) and SiH_2Cl_2 (dichlorsilane) is reacting to form Silicon Nitride on both sides of the wafer. The low-stress nitride is produced with a special recipe called *Sirich*, after which the oven will need cleaning due to particle formation.

HDMS (step 2.1 and 5.1)

Is done before spinning on photo resist, to promote resist adhesion on the Silicon Nitride substrate.

Spinning on photo resist (step 2.2 , 5.2 and 7.1)

In these steps, resist is spun on the wafer to be used for photo lithography. Liquid resist is applied, then the wafer is spun quickly and the resist will for a very thin layer.

(2.2) and (5.2)

In the first step (2.2) it is important to protect the wafer front side, both to avoid unwanted KOH etching, and to protect the nitride that will be forming the membranes. For this reason, the KS spinner, that has very gentle handling, is used.
In the second step (5.2), there are membranes on the wafer, and therefore the vacuum chuck cannot be used. If a membrane is broken there is a chance resist will get into the vacuum system so this is not allowed. Instead, a non-vacuum chuck is used, that holds the wafer in place with pins on the edges instead of vacuum.

(7.1)

The last resist spinning is done with a thicker resist to protect the membranes for the dicing.

Bake (step 2.3 , 5.3 and 7.2)

To harden the resist and evaporate solvent, the wafer is baked at 90^0C for 90 sec.

Flat alignment (step 2.4)

This is done in the KS aligner.
It is necessary to align the first mask to the wafer flat to make sure that the Si-crystal orientation is correct for the KOH etching. If the flat alignment is not correct, the membranes will end up having the wrong size.

Exposure, negative process (step 2.4 and 5.4)

Both lithography steps performed here are negative processes, so the steps to exposure the wafer are the same.
After the alignment is done, the resist is exposed with UV-light for 3.5 seconds. The mask is bright field, so the structures that will later be formed are protected from the light. After this, a so-called reverse bake is performed, meaning baking the wafer on a 120^0C hotplate for 2 minutes. The next step is a flood exposure, where the entire wafer is illuminated for 30 seconds and the final result is a negative process.

Development (step 2.7 and 5.7)

In this step, the resist is developed, meaning that the the resist that was not exposed in the first step is dissolved, thus forming the reverse image of the mask on the wafer.

RIE (step 3.1)

RIE is a reactive ion etch, where plasma of CF_4, H_2 and N_2 gasses is used to etch holes in the Nitride before KOH. This gas mixture will etch nitride, but not resist, so this acts as mask in the etching.

Plasma etch (step 3.2)

After RIE the remaining resist is cleaned off in the plasma oven in a O_2/N_2 mixture.

KOH (step 4.2)

KOH is used to etch all the way through the wafer, thus exposing the Nitride membranes on the front side.

Alignment for metal deposition (step 5.4)

In this step, the second mask with the metal structures is aligned to the membranes on the wafer using the alignment marks. A good alignment is quite important, especially for the pressure sensor that should be as symmetric as possible around the membrane.

Metal deposition (step 6.1)

The metal deposition is done by melting a metal with an electron beam and then leading the evaporated metal on to the wafer. In this case first a 10 nm layer of Titan and then a 50 or 100 nm layer of gold or platinum. The titanium is to improve adhesion to the nitride.

Lift off (step 6.2

Lift off is done in Acetone. It is important to do a negative photo lithography process to make sure that the metal edges are formed so the Acetone has access to the resist. Normally lift off is done in acetone with ultrasound, but in this case ultrasound must be turned off, otherwise the membranes will burst. This can mean a more tedious liftoff process to get all metal, especially the smaller structures, released.

3.1.1 Different versions fabricated

At project startup, 50 nm nitride was grown on 24 wafers. Wafers with 100 nm nitride already existed, and a few of these were used as well.
KOH etching was done on two batches, the first batch included two wafers with 100nm nitride and 4 wafers with 50nm nitride. From these one 50nm where only processed until step 4.2, and hereafter covered in 9.5μm resist and diced. These chips were used for AFM measurements and some work in the SEM. Of the last five, two 50 nm and one 100 nm were processed further with mask 2 for metal deposition. One 100nm and one 50nm were saved for later. Of the three processed further, 100 nm gold was deposited on the 100 nm membrane wafer, and on one 50 nm, while the last 50 nm had 50 nm gold deposited.
The second batch of six wafers with 50 nm Silicon Nitride where processed. This time, 3 of these where finished, two with gold, 50 and 100 nm, and one with 100 nm platinum.

3.2 Processing problems

Several problems arose during the processing, no serious set-backs, but a lot of small ones. In this section these problems will be described.

3.2.1 First batch

Development problems

The first time the metal layer mask was developed, problems where discovered. After development when the wafers where inspected in microscope, it was clear that there was bad adhesion between silicon nitride and resist. The problem was that the HMDS step had been skipped (forgotten..) and the necessity of the HMDS preparation was clearly demonstrated. The developed resist was removed in the plasma asher, and HDMS was done before spinning on new resist. This time there was of course no adhesion problems.

Alignment problems

In the alignment processes several problems were discovered.
To protect the nitride layer, a special chuck was used to hold the wafers. This only supports the wafer on the rim, and thus protects the wafer front side in the first alignment step. This system worked perfectly for the first mask alignment in the first batch, but already in the alignment of the second mask in the first batch some problems appeared. In the alignment, it seemed that the distance between mask and wafer was too large and it was impossible to bring both in focus. The alignment was done as good as possible and the exposure was done anyway, but the result clearly showed that the conditions had not been optimum. This caused the smaller structures to be distorted, the small structures were diffraction patterns rather than the shape of the mask, and the corners of the bigger structures where not clearly defined with diffraction like shapes. This is a clear sign that there had been a gap between wafer and mask during exposure. What caused this problem is not clear, but it might be the wafers, that for some reason were bending. To solve this problem it became necessary to use a vacuum chuck for holding the wafer. This solved the problem. The vacuum chuck has not been used in the first step, and it will have to be tested whether it will damage the nitride.

Broken wafers

In the cleanroom processing the first batch, it became apparent how fragile a 350 μm thick wafer is. One was completely lost, because it was dropped inside the spinner and another one broke when when it was lifted of the hotplate with a pair of tweezers. The first incident happened because the spinner was incorrectly programmed so it closed as the wafer was taken out. After this, wafers were handled even more gently and no more has broken.

Lift off

From the two 50nm wafers that made it all the way to lift off, the one with 50nm Au was destroyed. This happened when the ultrasound in the liftoff bath was turned on, which caused all nitride membranes to instantly burst. Therefore all other wafers went through the liftoff process without ultrasound.

3.2.2 Second batch

Allignment problems

In the second batch the problem with gap between wafer and mask appeared in the first alignment step, holes for KOH etching. This caused some of the membranes on each wafer to be smaller than intended, and others were even non-existing
A second problem in the alignment process where the flood exposure. For some reason the wafer was unevenly exposed and therefore the resist would not develop. This was eventually solved in the the second batch with mask2, by doing two flood exposures, the second one done with the wafer rotated 180° with respect to the first exposure. In the second batch the development of Mask 2 was far more successful than in the first batch and the lithography was perfect.

Lift off, sticky gold

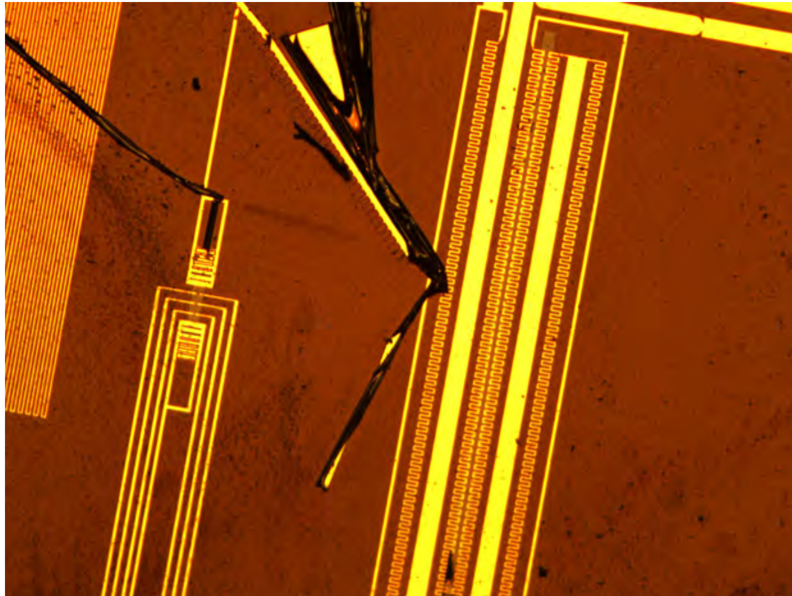

Figure 3.1: Picture of wafer with Au sticking to the surface after lift-off.

Another problem in second batch was in the liftoff, where the gold was sticking to the wafer in the liftoff bath, as shown in figure 3.1. This was less of a problem in the first batch, and might be due to the fact that the wafers were moved around in the bath, thus stirring up the gold that had come of the wafers. Also ultrasound might have been able to counter this problem. In a new batch, a long liftoff without moving the wafers and with good distance between them is recommended.

3.3 Sample holders

To make a good sample holder for the chips tuned out to be harder than expected.
To start with, a holder made by Kristian Mølhave, figure 3.2, was used. It is made of two parts, the first part is a block of polycarbonate, where two 1mm Ø holes are drilled all the way through the block. Each of these holes are connected to the sides of the block by valves. From beneath platinum wires are placed in each 1mm hole, and glued with epoxy.
The second part of the holder is a 1.5 mm thick PMMA plate, where a 3×3 mm^2 and 0.5 mm deep hole is burned with a CO_2 laser. A smaller 2×2 mm^2 hole is then burned all the way through, in the middle of the 3×3 mm^2 hole. The idea of this is that the 3×3 mm^2 first generation membrane chip, that was made prior to this project, will be easy to align correctly above the hole, when glued with epoxy. The two parts of the chip holder are then screwed together with a sealing in between.

Figure 3.2: Picture of chip holder made by Kristian Mølhave

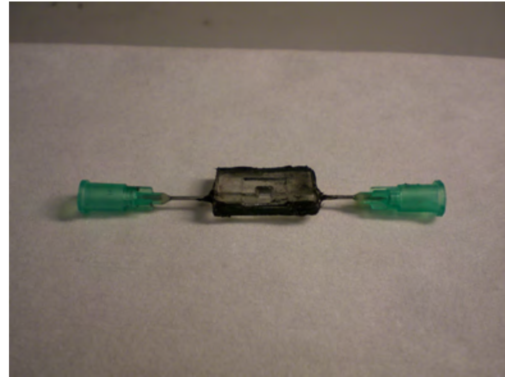

Figure 3.3: Picture of chip holder with needles. A problem with this type, is that it's hard to make tight around the needles. But haves advantages in being small enough to fit into AFM.

This kind of sample holder did have a few problems. One is that it's hard to make completely tight, often some leaking would appear. Another problem was the small sealing. The hight of this induced stress in the PMMA when the two parts were screwed together, stress that could lead to destruction of the chip. For this reason, several new designs were tested for the second generation chip produced in this project.

3.3.1 No-seal PMMA holder

The first one was made of two plates of PMMA, one with a channel in it, and the other one with a hole fitting the chip device area. These two plates where glued together with a needle in each side as seen in figure 3.3. After this, the chip could be glued onto the top of the holder. The idea behind this design was to make a very simple, but one-time use holder without seals, and therefore not stressing the plastic and avoiding the chips breaking. The problem about leaking was still present though, this was now from the needles, since their surface apparently has a very poor adhesion to epoxy, the needles could simply be turned around or even removed after the epoxy had set hard. We tried to cope with this problem by sandpapering the needles before gluing, which helped, but still tightness was only reached in a small portion of the holders. This design did have the advantage though, that it was small enough to fit into the AFM, used for measuring deflection of the membrane under pressure.

3.3.2 New generation of original holder

Because of the problems with the no-seal holder, another attempt was made with the original design, with some modifications though. First of all, the chip dimensions are different for the new chip, and the holder needed to fit this, as well as the attached ZIF socket, figure 3.4. A silicone sealing of heat resistant silicon glue was made directly on the polycarbonate block, and then a PMMA 'lid' was screwed on before the chip was glued. This method seemed to solve all the problems. It was tight, with no leaking and because the chip was glued onto PMMA after it was placed on the polycarbonate, the chip did not experience stress from the PMMA. This holder also have some flaws though. The biggest one is, that to make the ZIF socket fit, it had to be attached to the chip before the gluing, thus making reuse of the custom made double ZIF sockets(section 3.3.4) impossible.
This type of holder was used to test pressure sensor, thermistor and heater.

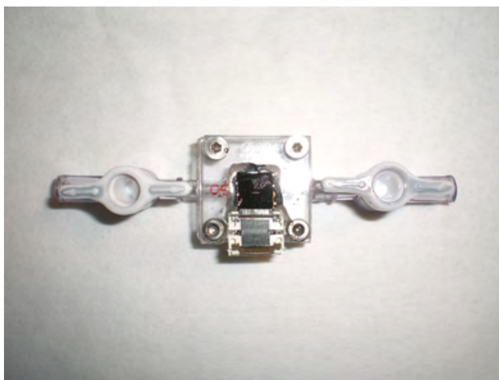

Figure 3.4: Chip holder of same type as KM´s, but adapted to fit ZIF sockets and larger chip. One problem with this holder is that the double ZIF socket is glued to the holder.

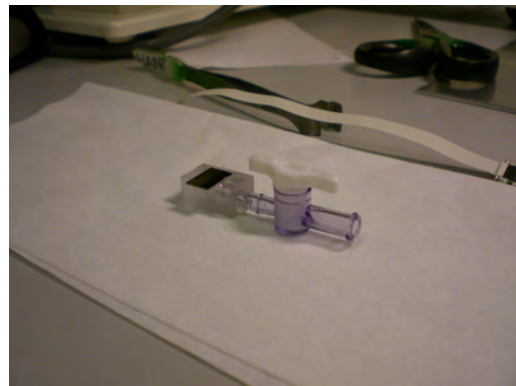

Figure 3.5: Picture of holder, where the chip is glued directly to the thick polycarbonate. The advantage of this holder is that it's easy to fill with liquid and the double ZIF socket can be changed.

3.3.3 "'Fill-easy"' holders

The last holder was made, after it was discovered how hard it was filling up the chip holder with liquid without having air bubbles present in the chamber at chip surface. Having contact between chip and liquid is obviously mandatory for the electro chemistry and SEM imaging to work.
For this reason, a new holder was made, shown in figure 3.5. This holder is easy to fill with liquid because it's possible to fill the chamber bottom up, and the small channels up to the chamber are removed. Another good thing about this holder is that it's possible to re-use the double ZIF socket, and it is possible to visually control if there are any bubbles on the chip. Of course this holder also has a problem; the chip is not supported where the ZIF socket is, and therefore it is very fragile, and easily breaks when one attach the socket.

Several designs have been proposed and tried, all with their own problems, and most likely if the work was carried on by us, we would attempt to make even another design, trying to combine the advantages of the different holders mentioned above, while minimizing the problems.

3.3.4 Connections, the Double ZIF socket

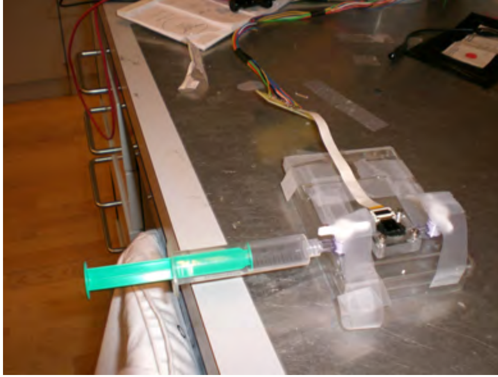

Figure 3.6: Picture of the full connection from chip to wires in pressure test setup.

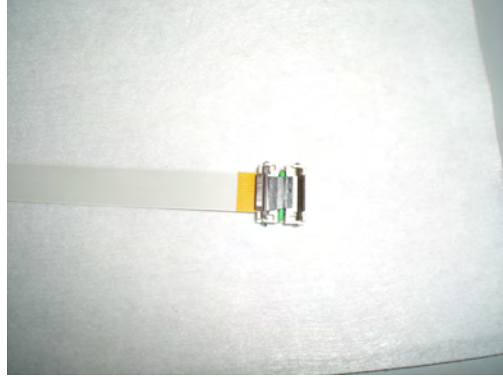

Figure 3.7: Picture of a double ZIF socket connected to ZIF wire. Used to connect chip, note that the double ZIF socket is enhanced with tape.

Figure 3.8: ZIF socket with kind of lock thats easy to fit the chip.

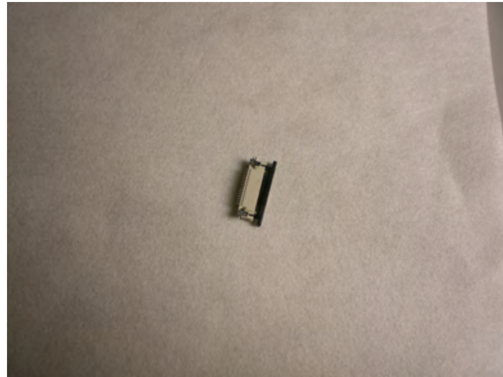

Figure 3.9: ZIF socket with kind of lock that often will break the chip.

For connecting the chip to a cable it was necessary to make our own double ZIF sockets, since these are strange enough not commercially available. These were made by soldering together two normal 16 pin ZIF sockets, as shown in figure 3.7. These where not very durable, so they where reinforced with epoxy or tape.. It was soon discovered though, that any epoxy on the soldered electrodes, would break the soldering in the hardening process. Different typed of ZIF sockets were tried, and the easiest one to place on the chip, was the type pictured in figure 3.8. The other type see fig.3.9 did not work as well due to the larger force needed to lock the socket, leading to a possible breaking of the fragile chips.
The double ZIF socket is attached to a special ZIF cable, that again is attached to a circuit board, on which cables are attached to allow external connections. The entire setup is pictured in figure 3.6.

3.4 Yield

The yield of the ending product has been quite low, because of all the problems in the processing and with the sample holders.
In the cleanroom plenty of chips were lost or not all devices were working, due to the problem mentioned in section 3.2. A lot of this though, has been due to us being inexperienced,

and the chances are good that a new batch could be produced with a much higher yield. One problem seems to be persistent though, and that is thermistors not working. Because of this, many otherwise good chips had to be scrapped. The reason for this bad yield is seen in figure 3.10, and that is, that the thermistor, covering such a big area with thin wires, is very vulnerable to dust contamination. For this reason it is suggested to explore the possibility of adding a cleaning step before doing the second lithography. This was not done out of fear of destroying the membranes, but a few broken membranes might be a good trade off for a higher yield of the thermistors.
A lot of chips where also lost when glued to the chip holder, either because glue got onto the central parts of the chip, or because the chip broke. In the type of chip holder seen in figure 3.4, where the double ZIF socket is glued onto the holder, the soldering might break, and loose contact, and both chip and holder is lost.
The other problems are quite different, here the solution have to be to make a chip holder where it's easy to place the chip, and still make it pressure tight.
All that being said, it is our opinion that the membranes themselves have been very robust

Figure 3.10: Picture of thermistor broken by dust particles.

during the processing, and when a working chip is been correctly attached and connected, it is a reasonably sturdy system.

4
Results

4.1 AFM measurements of membrane deflection

As part of the project, atomic force microscopy, AFM, was used to investigate the membrane deflection. AFM measurements was done at Nanoteket, DTU.
Two chips were tested in AFM, both was with 50nm membrane, one with and one without the gold layer. First deflection of the clean 50nm membrane was measured. This was done by connecting a syringe to the chip holder and to a Honeywell pressure sensor.
The pressure was changed in small steps and in each step a picture of the membrane was recorded. The picture is then analyzed using the EasyScan software as shown in figure 4.1, and the height of the membrane is found at three locations for each pressure.

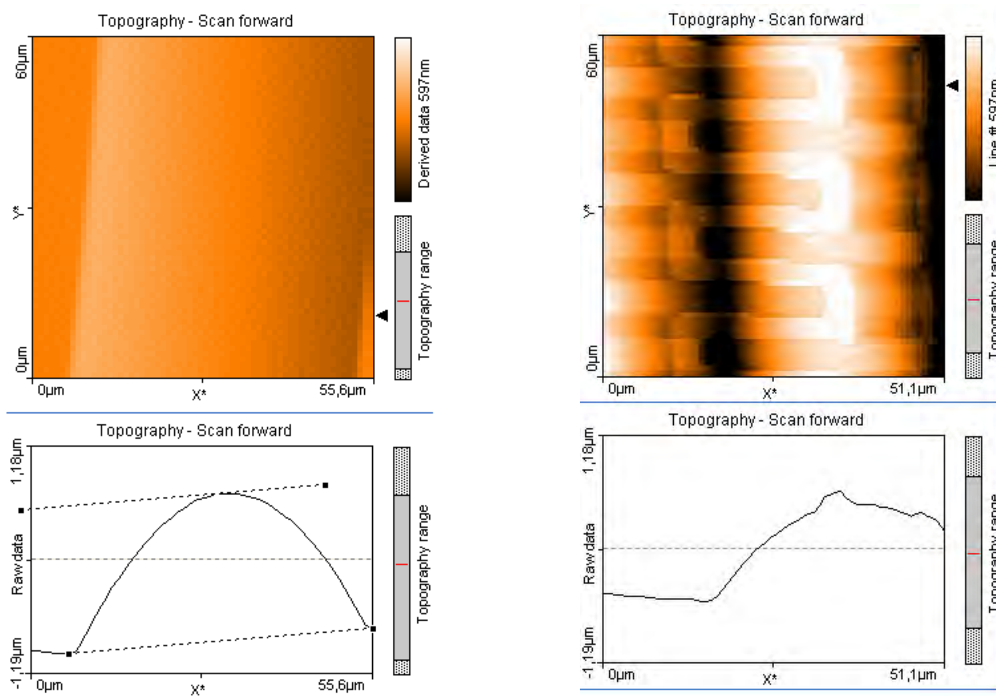

Figure 4.1: Pictures from Easyscan showing a clean 50nm membrane under 1.5 bar pressure together with a cross sectional plot, used to measure the deflection.

Figure 4.2: Same picture as figure 4.1, but with 100nm thick Au wires.

Three heights from each picture are found and used to find an average height witch is plotted in figure 4.3. Here it is clear that the height of deflection is not linear with pressure, and that the gold has an effect on the maximum deflection.
It should be said that the results here might be slightly off from the actual value. When

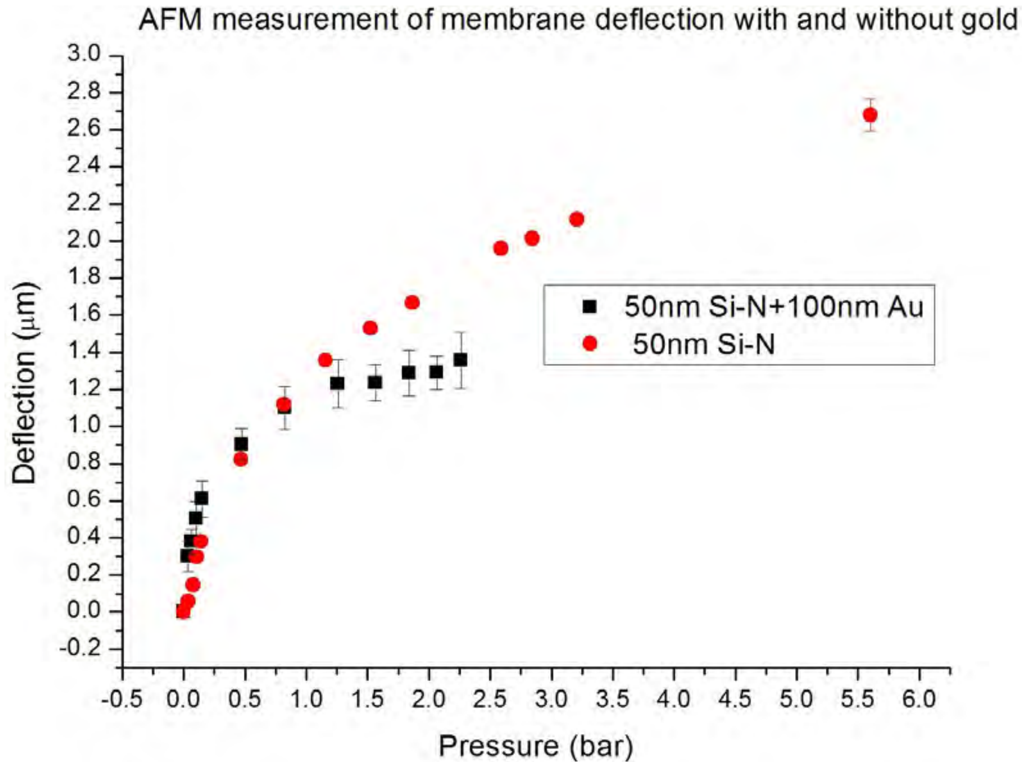

Figure 4.3: Plot of the deflection of the membrane at different pressures

analysis was performed after measurements it was clear that it would have been preferable to have the full membrane and a part of both plane sides within the scan range. This would have made it possible to lay a more accurate baseline to measure the deflection from. This problem is illustrated in figures 4.4 and 4.5.

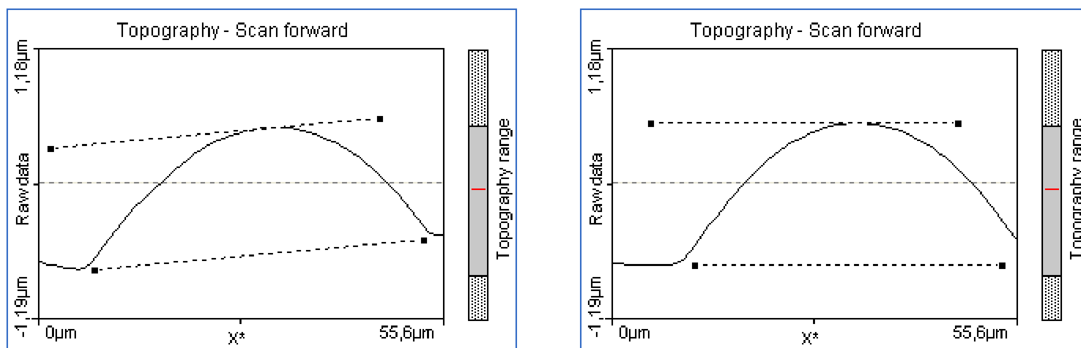

Figure 4.4: Both plane sides is in the scan range, so a base line is easily placed to measure the deflection

Figure 4.5: Here the position of the baseline will be more of a guess, because both plane sides are not within the scan range.

4.1.1 Membrane fracture

After the AFM measurements it was decided to try breaking the membrane. Inside the AFM the pressure went as high as 5.6 bar, but the membrane was tested to even higher pressure. In fact as high as it was possible to push the piston with by hand. The Honeywell is calibrated to 6.7 bar, and supposing the linearity holds till it caps out, the pressure was

as high as 8 bar, without the membrane bursting. This is far higher than the fracture pressure suggested in the design chapter and suggests that this nitride is very durable.
Doing real fracture tests on different thicknesses and comparing with the model for large deflection would be very interesting.

4.1.2 Fitting to AFM

The data acquired in the AFM can be fitted to the model presented in section 2.2.4, and in this way, Young's modulus and the build-in stress can be determined.
Because of the non-linearity of the model, it is not possible to directly fit the function. Instead it is done in Matlab, complete code listing is seen in Appendix 2.
To recap, the maximum deflection w_0, measured by AFM is in transformed coordinates described by equation 4.1.1. This one however, is dependent on $\bar{s}$, that again is dependent on w_0. This means that to find w_0 as function of pressure, one needs to solve equation 4.1.2 numerically first.

$$\bar{w_0} = \bar{P}G(\bar{s}) \tag{4.1.1}$$

$$\bar{s} = \bar{s}_0 + \frac{1}{2} \cdot \bar{w}_0^2 \cdot H(\bar{s}) \tag{4.1.2}$$

The two fitting parameters are the plain-strain modulus E_{ps} and the build-in stress s_0. It has been chosen though, to give Young's modulus E as output of the fitting, which means that Poisson's ration ν has been set to 0.23, and E is found according to $E_{ps} = E/(1-\nu^2)$.
A function called `fitfun` is created, which takes the inputs `param, P, w0, h, width` where `param` is a vector containing values for `Eps` and `s0`, `P` and `w0` are vectors containing the experimental values and `h` and `width` are the dimensions of the plate. For a set of input values, `fitfun` will take the deflections `w0` and calculate $\bar{s}$ according to that. When this is calculated, it is inserted in equation 4.1.1 and w_0 is calculated (from $\bar{w_0}$) and compared with the experimental value. Notice that the unit used for w_0 is μm. The function output is the sum of these squared errors, or the mean squared error of the fit.

Finally, in the function `fitmem`, the build-in Matlab function `fminsearch` is used to minimize `fitfun` with respect to `Eps` and `s0`. Finally the experimental values are plotted together with the model values for the deflection with the found parameters, as can be seen in figure 4.6. The values found, are actually noticeably different from the values used in the calculations and simulations presented earlier. Here, Young's modulus was set to 255 GPa, while no initial stress was taken into consideration. From the AFM measurements values are found to be:

$$E = 132 \text{ GPa} \tag{4.1.3}$$

$$s_{build-in} = 258 \text{ MPa} \tag{4.1.4}$$

This is with all points, and the mean squared error take the value 0.0196. If instead the last point is omitted, this error changes to 0.0131 and it gives $E = 137$ GPa and $s_{build-in} = 245$ MPa
When considering figure 4.6 one can see that the model as well as the found fitting parameters seem to agree quite well with the observed deflection. The Young's modulus is noticeably low compared to the previous value taken from literature, and the build in stress is also a bit higher than the designed value of 100 MPa (according to supersvisor Torben M. Hansen). If this is wrong, it must be due to the AFM-measurements, since the error of the fit is so small. This also means, that if the measurements are wrong, then the error

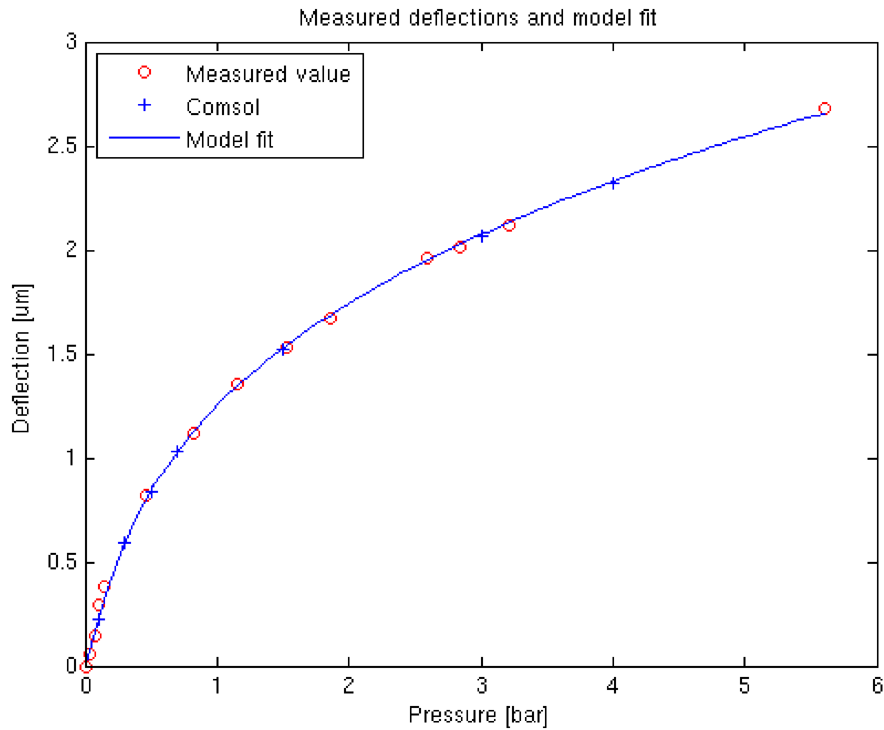

Figure 4.6: Large deflection model is fittet to the experimental values for the deflection. In this way, Young's modulus E and the build-in stress s_0 are found.

must be very systematic. As previously stated, the AFM might be used a bit differently to give higher accuracy, and this is definitely suggested if the found values are to be used as reference in the future.
All that being said, a quick and easy-to-use technique has been applied to determine the plain-strain modulus and build-in stress of the low-stress silicon nitride, as first demonstrated by [Yang and Paul, 2002].
As a test of the Comsol modeling of the membrane, values found using the software with the new values for E and s_0 is also plotted in figure 4.6 and is in perfect agreement with experiment and large deflection model.

4.2 Calibration of the thermistor

To test the thermistor a chip was placed in an oven connected to a multimeter through the ZIF socket. Very close to the chip a thermocouple was placed to measure the temperature. The oven was then heated up in steps of 5°C, where in each step time was given for the temperature to stabilize. The resistance of the thermistor was then recorded together with the temperature as measured by the thermocouple. The setup is shown in figure 4.7.
Two chips where tested, one with 100 nm gold and one with 50 nm gold.

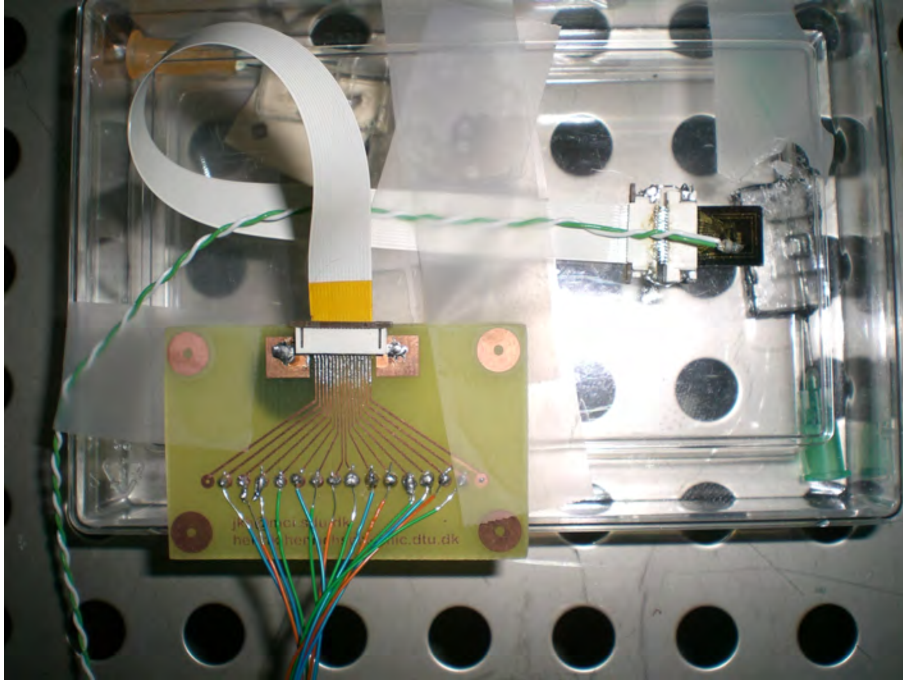

Figure 4.7: Setup used to test and calibrate the thermistor

4.2.1 Data

In figure 4.8 and figure 4.9 plots of resistance vs. temperature for 50nm and 100nm Au thermistor are plotted.
As can be seen, the response is nice and linear, with a clearly measurable response, -just as predicted by theory. The fits to the data points are:

$$R(T) = 26.37\frac{\Omega}{^o\mathrm{C}} \cdot T + 12341\ \Omega \quad \text{for the 50 nm Au} \tag{4.2.1}$$

$$R(T) = 15.77\frac{\Omega}{^o\mathrm{C}} \cdot T + 6289\ \Omega \quad \text{for the 100 nm Au} \tag{4.2.2}$$

To recap from the previous section, the linear resistance dependence on temperature for a metal can be described by the equation

$$R(T) = R_0(1 + \alpha(T - T_0)) \tag{4.2.3}$$

$$R(T) = R_0(1 - \alpha T_0) + \alpha R_0 T \tag{4.2.4}$$

Where α is the temperature coefficient of electrical resistance at T_0 and R_0 is the resistance at T_0

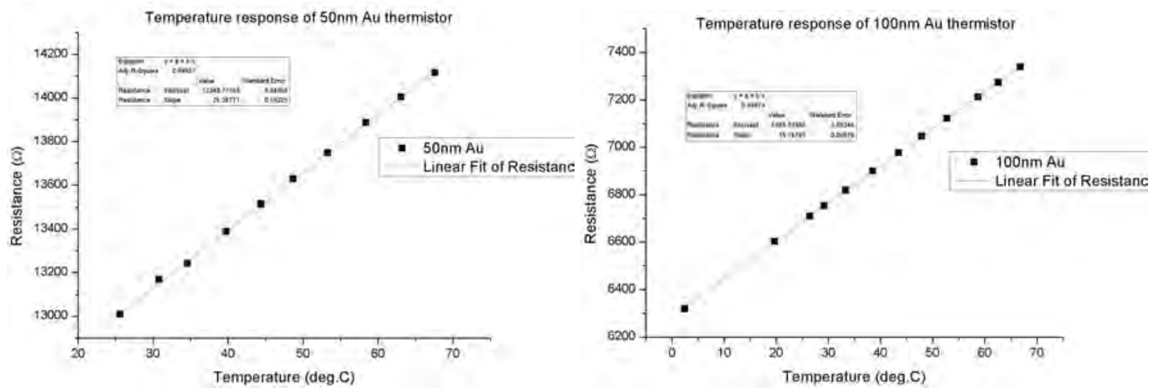

Figure 4.8: Plot of the resistance vs. temperature for 50nm Au thermistor

Figure 4.9: Plot of the resistance vs. temperature for 100nm Au thermistor

The gathered data now makes it possible to determine α for these samples. Since a reference value is known at $T_0 = 20^o$C this α will be determined here.
The calculations are shown for the 100 nm Au chip.
Using formula 4.2.2 one can calculate R_0 (meaning resistance at 20^oC) to 6604 Ω. Then the second term of equation 4.2.4 is used together with equation 4.2.2 to determine α according to:

$$\alpha R_0 T = 15.77\frac{\Omega}{^0\mathrm{C}} \cdot T \quad (4.2.5)$$

$$\alpha = \frac{15.77\frac{\Omega}{^0\mathrm{C}}}{R_0} = 0.00239\mathrm{K}^{-1} \quad (4.2.6)$$

and for 50 nm Au

$$\alpha = 0.00205\mathrm{K}^{-1} \quad (4.2.7)$$

The bulk value used in the design calculations was α=0.0034K^{-1}.

4.2.2 Theory of conductance in thin metal films

When comparing then actual results with the expected, it is obvious that the thermistor does not behave as expected in the design phase, both resistance and the temperature coefficient of resistance are much different from the expected values. In the previous calculations, bulk values where used for resistivity and temperature coefficient, and this assumption is clearly not valid for 50 and 100 nm thin films. For this reason, we will look a bit more into how thin films behave electrically, and how the equations used as foundation for the design might be corrected.
At room temperature, the resistivity of metals is governed by the scattering of electrons on thermal phonons, and the resistivity can be described as function of the quantity 'electron mean free path' λ_0. λ_0 is defined as the mean distance an electron can travel in the material without being scattered. What happens in a thin film, is, that as the thickness approaches λ_0, electron scattering on the surface of the film will become more and more dominant, which leads to a decrease in conductivity.
The bulk conductivity σ_0 in a system of N free electrons per unit volume can be written

as:

$$\sigma_0 = \frac{Ne^2\lambda_0}{mv_F} \quad (4.2.8)$$

$$\Downarrow \quad (4.2.9)$$

$$\lambda_0 = \frac{\sigma_0 m v_F}{Ne^2} \quad (4.2.10)$$

where e and m are electron charge and mass and v_F is Fermi velocity.
The values for these numbers are:

$$\sigma_0 = 4.88 \cdot 10^7 \Omega^{-1}\text{m}^{-1} \quad \text{at } 20^o\text{C} \quad (4.2.11)$$

$$m = 9.11 \cdot 10^{-31} \text{ kg} \quad (4.2.12)$$

$$e = 1.602 \cdot 10^{-19} \text{ C} \quad (4.2.13)$$

$$N = 5.9 \cdot 10^{28} \text{ m}^{-3} \quad (4.2.14)$$

$$v_F = 1.4 \cdot 10^6 \text{ ms}^{-1} \quad (4.2.15)$$

conductivity from [CRC, 2008], other values from [Young and Budynas, 2005].
From this it can be calculated that $\lambda_0 = 41.1 \cdot 10^{-9}$ m, and the film thickness t to λ_0 ratio is 2.4 and 1.2 for 100 and 50 nm gold respectively.
[Heavens, 1973] treat the subject and the following will be based on this book. For the conductance of films, the author distinguish between thin and thick films, where for thick films $\frac{t}{\lambda_0} > 5$ and for thin films $\frac{t}{\lambda_0} < 0.1$. Clearly, the films treated here, do not fall into these any of these categories, and no valid approximation is presented.
The model for very thin films give no valid result for these thicknesses, but the thick film model

$$\sigma = \sigma_0 \left(1 - \frac{3\lambda_0}{8t}\right) = \sigma_0 \cdot X \quad (4.2.16)$$

gives $X = 0.85$ for the 100 nm film and $X = 0.69$ for the 50 nm film. For the measured resistances, it must be true that

$$\frac{R_0}{R_{Thinfilm}} = X \quad (4.2.17)$$

Where $R_{Thinfilm}$ is the resistance measured at a certain temperature and R_0 is the expected bulk value at that temperature. The actual ratio between designed and measured values are around 0.52 and 0.54 for 100 and 50 nm respectively. This lies in between typical values for the thick and thin films as presented in [Heavens, 1973] (page 117). One would expect X to be smaller for 50 nm than for 100 nm, but probably the difference is so small, that it is easily over shadowed by variations in the process (like a metal deposition slightly smaller or bigger than the desired). This also mean that calculating the resistance accurately on beforehand is close to impossible, though it seems using a resistivity of roughly twice the bulk value, would be a good starting point in the design phase.
For the temperature coefficient of resistance α a similar effect can be observed, if α_F is the thin film value, and α_0 is the bulk one, then the equation

$$\alpha_F = \left(1 - \frac{3\lambda_0}{8t}\right) \alpha_0 \quad (4.2.18)$$

should describe the relationship in good agreement with experiment for t/λ_0 around 4-5 according to [Heavens, 1973]. Again this ratio is lower in the present case, and the

model will overestimate the value for α_F, as is seen from the results of equation 4.2.18: α_F=0.0029K^{-1} and α_F=0.0024K^{-1} for 100 and 50 nm respectively. Experimental values where 0.0024K^{-1} and 0.0021K^{-1}, that is lower than the model. Here though, in agreement with theory, a lower value has been observed for the 50 nm thin film.
It has been shown that the thermistors respond linearly to temperature, and is working as intended. Values for α were extracted, and some theory of conductance in thin films has been applied to explain why the observed values for conductivity and temperature coefficient were lower than the bulk values used in the design phase. All in all the thermistor is working as intended and is a usable sub-device on the chip. A calibration of each chip might be recommendable, at least until more chips has been tested and there is a better statistical foundation. R_0 would always vary for different chips, but if α turns out to be consistent, then a general expression could still be made where only the resistance in a single temperature is needed instead of a more cumbersome calibration.

4.3 Pressure sensor measurements

The next sub-device to look at is the pressure sensor. Two chips where tested, showing quite different behavior. Both were from "‘Batch one"’ and with 100 nm gold metal layer. The first chip, denoted "‘chip1"’, was behaving very strangely, reacting totally unexpected to temperature changes. The second one tested was responding more as expected and the main effort was placed here. It cannot be said that chip2 was acting in a more correct way, but the results simply seemed to make a lot more sense, as shall be seen in the following. Both chips was tested in both positive and negative pressures, but since it is designed for positive pressures (higher pressure at the metal side), and this is what the chip will experience in the SEM, more focus has been here. For chip2, negative pressure was only applied late in the test process, after data had been acquired for positive pressures.

4.3.1 Test setup

The chip was installed in a sample holder and set of with connections to heater, temperature sensor and pressure sensor, in addition to pressure control.

Voltage control and monitoring

The voltage control and monitoring was done using a lock-in amplifier, that can supply an alternating current as well as measuring one. This is ideal for the Wheatstone bridge setup, where input voltage V_S is needed on the bridge as well as monitoring output. V_S was set to 1.5 V and set on gate 9 and 11 (see table 2.3), and the output voltage, V_{out} was then measured between gate 8 and 10.
In the rest of this chapter V_{out} will be referred to as simply the voltage, and sensitivity will refer to the slope of the voltage versus pressure relationship. The reason that V_S is chosen to be 1.5V is that V_{out} was 100 mV and the precision of the lock-in could be set to 100 mV, instead of 500 mV, that would have been necessary was V_{out} higher. On the other hand, a lower V_S would mean a lower output, so 1.5 V is the 'sweet spot' in terms of sensitivity and signal strength. Notice here, that a 100 mV output at zero pressure means an unbalanced Wheatstone bridge, contrary to what was designed. When a chip was connected, the lock-in was set adjusted to set the initial readout as an offset, so it would show $V_{out} = 0$ V at zero pressure. So when in the following a voltage is mentioned, the actual voltage is this plus the off-set.

Pressure control

The pressure was applied using a syringe connected to the chip holder. The pressure was monitored with a commercial pressure sensor from Honeywell, with a response of 40 mV/Psi and a range of 100 Psi (6.7 bar).

It has been chosen to fit a linear model to the responses, which, in the measured interval, seems like a reasonable approximation, as can also be seen from the displayed figures in this chapter.

4.3.2 Chip1, strange behaviour

As mentioned above strange behavior was observed for chip1, which was the first chip to be tested in the pressure setup. At first the voltage changed from negative to positive when the pressure changed sign, as can be seen in figure 4.10. This was similar to what was later seen for chip2, but with a higher response or sensitivity.

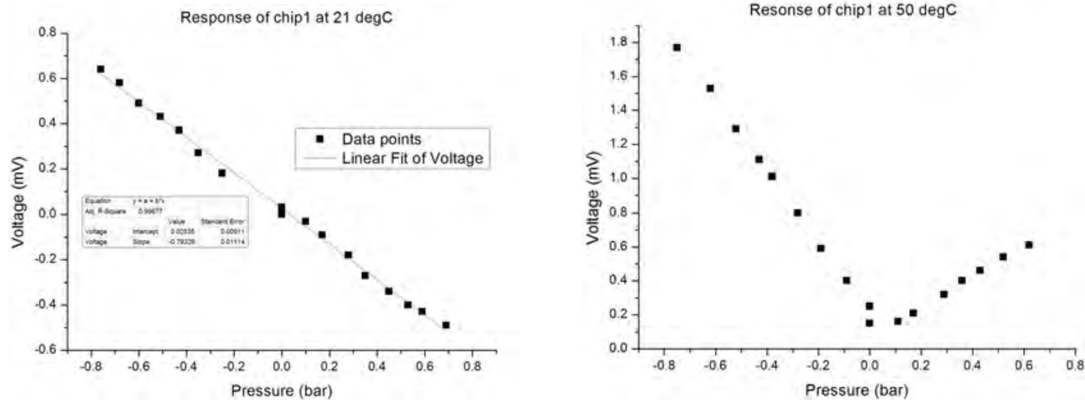

Figure 4.10: Response of chip1 at room temperature. Seems nice and linear across P=0 bar.

Figure 4.11: Response of chip1 at 50^{0}C. A very strange behavior. The voltage do not change sign across P=0 bar.

It was then decided to heat up the chip to see how that would affect the response, and it is here that the strangeness enters. For positive pressures, the direction of the response would now change, as seen on the plot shown in figure 4.11. After this, the chip was cooled down, and the behavior was again as in figure 4.10, so this shift was reversible.
The result was seriously puzzling and hard to explain. The similar response for both pressure directions was expectable due to the fact that the strain on the membrane (away from the edges) must be roughly the same for both pressure directions. On the edge of the membrane the sign of the strain must depend on the direction of the pressure, but only for negative pressures should a compression be observed, which might change the direction of the response.
Another thing observed for chip1 was a high latency. When a new pressure was set, it took a long time before the voltage would stabilize, maybe suggesting a plastic deformation. All i all these results where highly confusing, and it was decided to try another chip from the same batch, namely chip2. As it turned out, this one was behaving totally different, and no more effort was put into chip1.

4.3.3 Response at constant temperature

The first measurements were done, simply by variating the pressure at room temperature. Here it was seen, that the offset value for the voltage was not stable when the pressure was sweeped up and down repeatedly as shown in figure 4.12, which of course poses a problem in terms of reliability for the pressure sensor. This effect was seen through all measurements on both chips, the off-set voltage was not stable, suggesting irreversible effects taking place. What figure 4.12 also tells though, is that the slope is not varying too much between the sweeps, and slopes can be extracted from plots like figure 4.13. What this plot also suggests is that the difference between sweep directions is less pronounced for the pressures above 1 bar. Different values for the sensitivity at room temperature of both chips are compared in figure 4.14. Here one can also see how the sensitivity of chip1

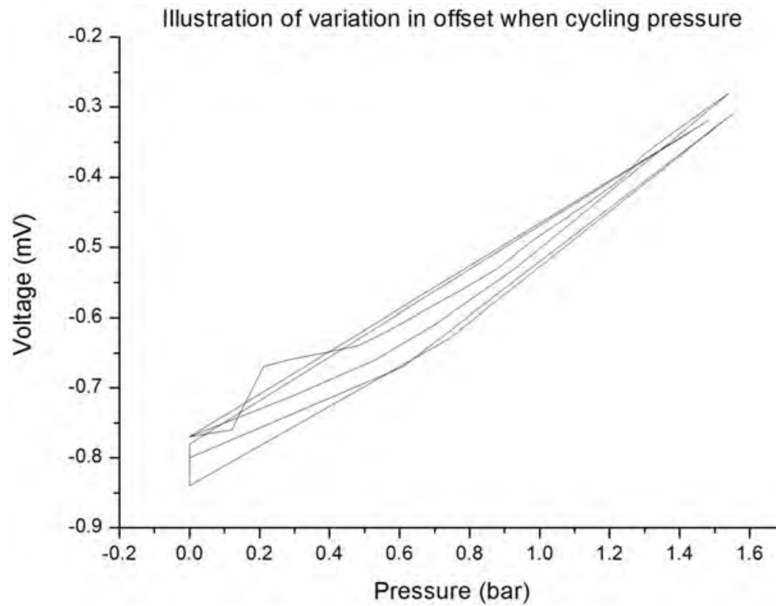

Figure 4.12: V-P measurement of chip2 at room temperature, showing how the offset changes when the pressure is sweeped up and down. Note also the slope is close to constant in each sweep.

would be different after it was heated, though still with the same sign. Apart from that,

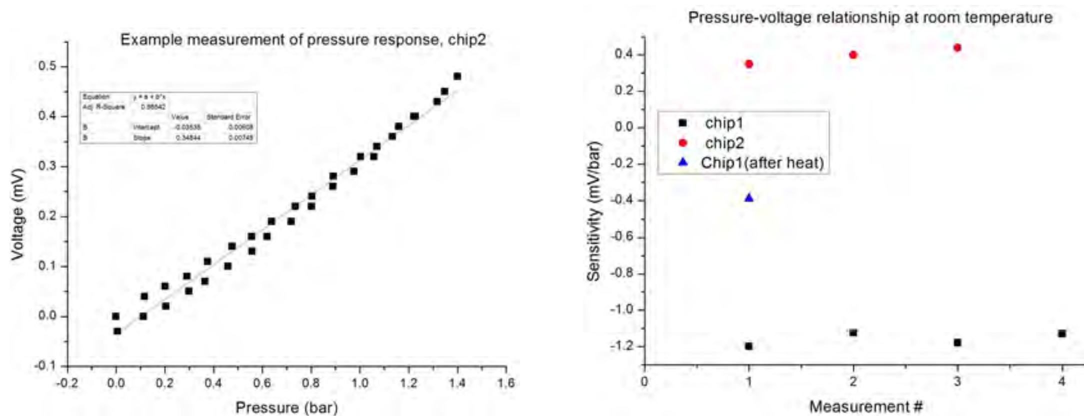

Figure 4.13: Voltage vs. pressure for chip2 at room temperature. P starts at 0bar, moves to 1.5 bar and down again.

Figure 4.14: Graph showing the slope in several measurements on each chip, all at room temperature.

it seems that the slopes are pretty stable for a number of measurements. If the magnitude of the sensitivity of the two chips are compared, it is seen that for chip1 it is remarkably bigger prior to the heating, whereas it has roughly the same magnitude as chip2 after. The mean sensitivity for chip2, based on the results shown, is $\langle a \rangle = 0,3966\text{mV/bar}$.

4.3.4 Varying temperature

It is expected that the temperature will have an effect on the offset. If there is a slight imbalance in resistors of the bridge, the temperature response will also be slightly different. It is also possible to imagine that the stress induced by discrepancy in thermal expansion coefficient on the membrane will be different from that on the silicon supported nitride. The sensitivity however, should stay constant at different temperatures. Figure 4.15 is

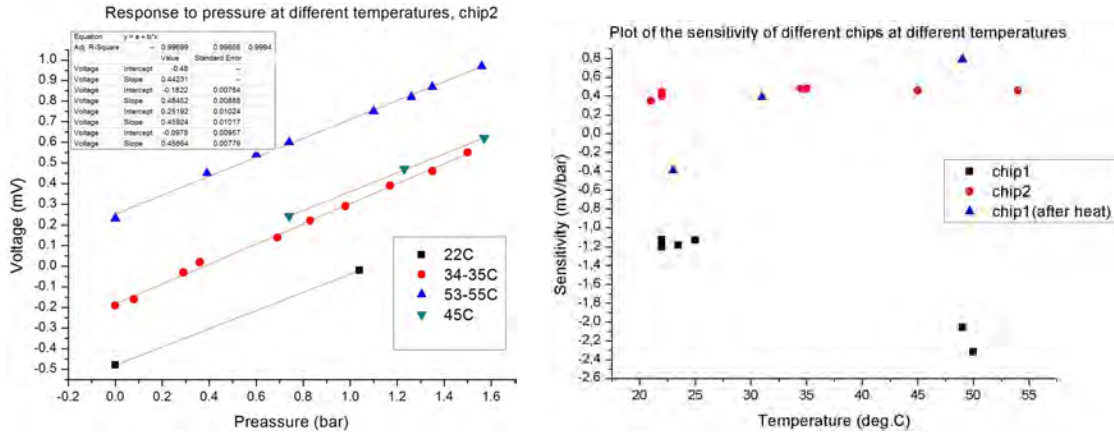

Figure 4.15: Response at different temperatures for chip2. It's seen that the offset depends of temperature, but the sensitivity is constant.

Figure 4.16: Data of sensitivities at different temperatures for both chips. Chip2 shows good compliance with expected behavior, while chip one have clear temperature dependency of the sensitivity.

a nice round of measurements showing similar slopes at different temperatures. Here, a pressure cycle has been run, then the temperature was changed and another cycle done once the temperature was stable. The chip's build-in heater was used to control the temperature with voltages between 1.5 and 6 V. Linear regressions have been done for all these temperatures, and the data is plotted in figure 4.16 together with values for a similar experiment for chip1. The average of the slopes is $\langle a \rangle = 0.4386 \pm 0.0478 \text{mV/bar}$ where the $\pm 0.0478 \text{mV/bar}$ is the standard deviation. Apart from showing that the slope remains

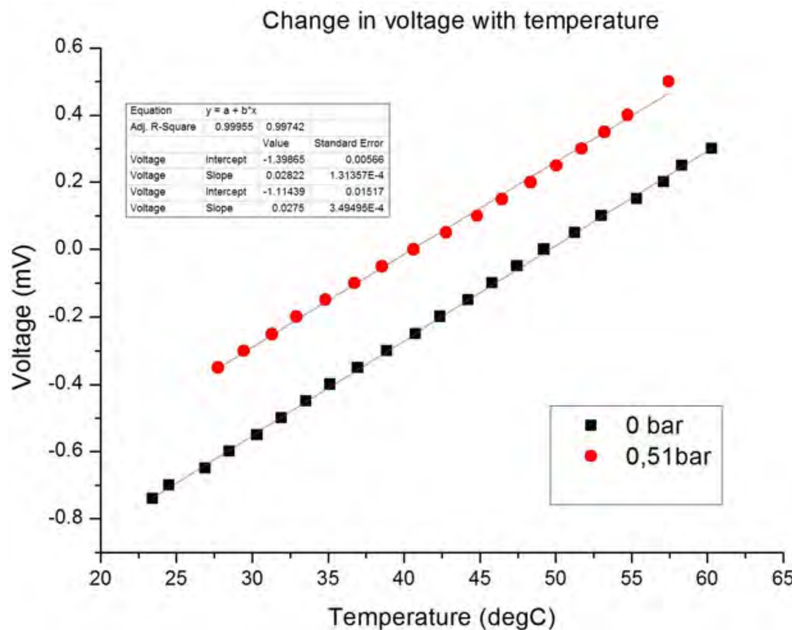

Figure 4.17: Plot of the voltage change due to temperature at different pressures. First the offset voltage was measured (0bar), then at 0,51 bar.

the same throughout the measured temperatures, figure 4.15 also displays what must be a change in the offset voltage as function of temperature. To explore this further, another experiment was set up, this time recording output voltage as function of temperature for two different pressures, the result is shown in figure 4.17. A linear behavior is observed,

and the slope seems to be more or less independent of the pressure, being close to 0.028 mV/^{o}C in both cases.

4.3.5 Modulating data

It was discovered, that in the measurements done on chip2, the linearity seemed to disappear at low pressures, and the measured voltages seems higher than they should be. It is proposed that the stabilization time is longer at low pressure, and therefore, in the measurement shown in the figure 4.18, the sensor was not given enough time to reach the stable voltage. This assumption is also based on the fact that for zero bar, two values have been recorded, one just after the pressure was released and one some time after, and the voltage dropped between these two times of measurement. Based on this observation, the data points, thought to be false are removed, and the fit is suddenly much better. This plot can be seen in figure 4.19

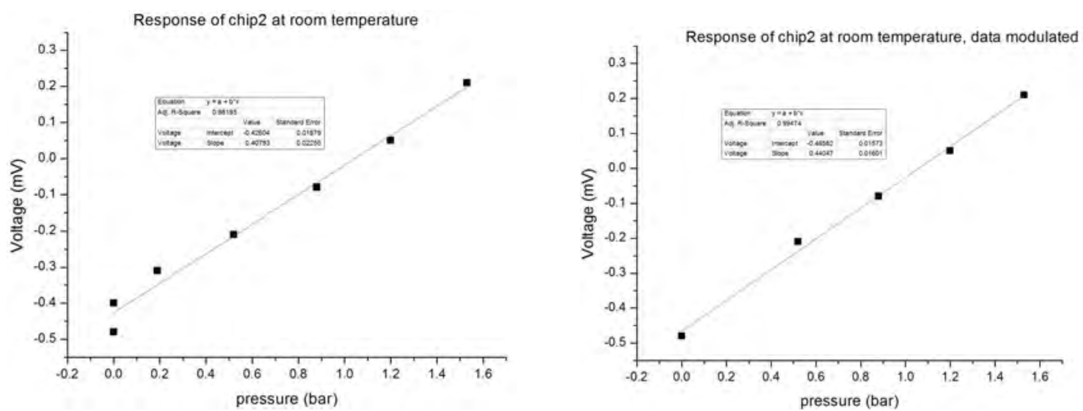

Figure 4.18: Voltage vs. pressure for chip2 at room temperature. P_{start}=1.5bar $P_{end} = 0bar$, P=0 points are taken just after pressure drop, while the second is taken after some time.

Figure 4.19: Same as figure 4.18, except here two one of the points are removed due to relaxation problems.

Now, the same thing is done to all data series, and the new, modulated, slopes shown in figure 4.20. The mean value for the sensitivity is now $\langle a \rangle$=0,45±0,03mV/bar, so a slightly higher value than seen in figure 4.14, and with a lower standard deviation.
This also suggests that some relaxation time is needed, at least when measuring lower pressures.

4.3.6 Summing up of the pressure sensor data.

From the data it seems reasonable to assume that only chip2 worked as intended. No definitive answer can be given to the reason for the behavior of chip1. Possible effects in play could be delamination of the metal, cracks in the metal or something else. Of course, more chips should be tested to give a better answer to what is actually normal or expected behavior, for all we know, the remaining chips might behave as chip1.
Hoping that is not the case, and that chip2 is representative, the summary for the pressure sensor can be summed up:

- The sensitivity of the pressure sensor is independent of temperature, and takes a value of $\langle a \rangle$=0.45±0,03mV/bar provided some time is allowed for stabilization. This is 0.045 mV per 0.1 bar, and based on this, the requirement set up is fulfilled.

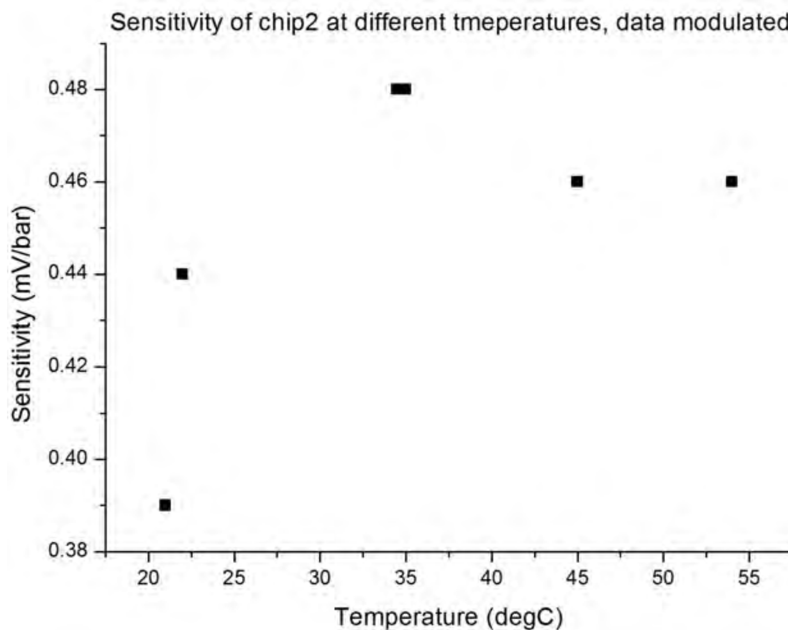

Figure 4.20: Modulated sensitivities of chip2 at different temperatures.

- The offset voltage is linear with temperature, and at 0bar V_{offset}=0.028mV/^{0}C·T-1.1144mV
- The offset voltage have stability problems if the pressure is swept up and down repeatedly.

Supposing that the problem of jumping offset and relaxation time was not present, it would be possible to develop a formula giving V_{offset} as function of pressure and temperature as:

$$V_{out} = 0.45\frac{\text{mV}}{\text{bar}} \cdot P + V_{offset} \tag{4.3.1}$$

$$\Updownarrow \tag{4.3.2}$$

$$P = \frac{V_{out} - V_{offset}}{0.45\frac{\text{mV}}{\text{bar}}} \tag{4.3.3}$$

$$V_{offset} = 0.0025\frac{\text{mV}}{^o\text{C}} \cdot T - 1.1144\text{mV} \tag{4.3.4}$$

$$\Downarrow \tag{4.3.5}$$

$$P = 2.2222\frac{\text{bar}}{\text{mV}} \cdot V_{out} - 0.0056\frac{\text{bar}}{^0\text{C}} \cdot T + 2.4764\text{bar} \tag{4.3.6}$$

The data recorded on the pressure sensors probably gives rise to more questions than it answers, and it is obvious that a lot more data is needed in order to be able to use this sub-device for accurate measurements. The strength of the signal is very week, though strong enough to fulfill the goal of reaching 0.1 bar precision. Because of the offset voltage of 100mV it was not possible to reach higher precision with the lock-in, but it is possible to imagine a construction of the Wheatstone bridge, where a variable resistor is placed outside the chip circuit, allowing for fine tuning of the resistance to reach an output of 0 V at 0 bar, in that case, it might be possible to measure with nanovolt precision.
That being said, it has been demonstrated that it *is* possible to see a meaningful response from a pressure sensor constructed as a strain gauge on top of a thin nitride membrane,

and it is definitely an approach that should be further investigated.

4.3.7 Another approach to simulating strain

In the design phase, only positive pressures where considered, and a response of 0.64mV/bar was predicted for the pressure sensor in the "mean strain approximation". As was seen from the results presented above, this estimate was higher than the actual one of 0.45mV/bar.
A simulation has also been carried out using the new value for Young's modulus and considering the build-in stress. This simulation though, gave a response of 0.79mV/bar, even further from the experimental value. It is not such a big surprise though, a lower Young's modulus as was found by the AFM measurements, will give a higher deflection and in the simulations cause a greater strain.
The next thing to consider is the validity of considering only mean strain, and here we will briefly present another way of modeling it.
It is not possible for Comsol to take into account geometrical changes due to strain, but the resistivity of a material can be changed as function of strain. In Comsol the conductivity of gold is set as $\sigma = 45.6 \cdot 10^6/(1+\gamma\epsilon_L)(\Omega\text{m})^{-1}$ where $\gamma = 2.32$ is an estimate of the gauge factor for gold as seen in section 2.4.1. If considering a very small part of the material with a uniform strain ϵ_L and with a resistance R in the non strained case and $R+\Delta R$ in the straianed case, then

$$\begin{aligned} R+\Delta R &= R(1+\gamma\epsilon_L) &(4.3.7)\\ &= constant \cdot \rho_0((1+\gamma\epsilon_L) = constant\rho(\epsilon_L) &(4.3.8) \end{aligned}$$

where *constant* is a term describing the geometry of the material piece and ρ is the resistivity. Since the conductivity is the inverse of the resistivity, it must be true that the strain dependent conductivity is described by $\sigma(\epsilon_L) = \sigma_0/(1+\gamma\epsilon_L)$ The result of this simulation,

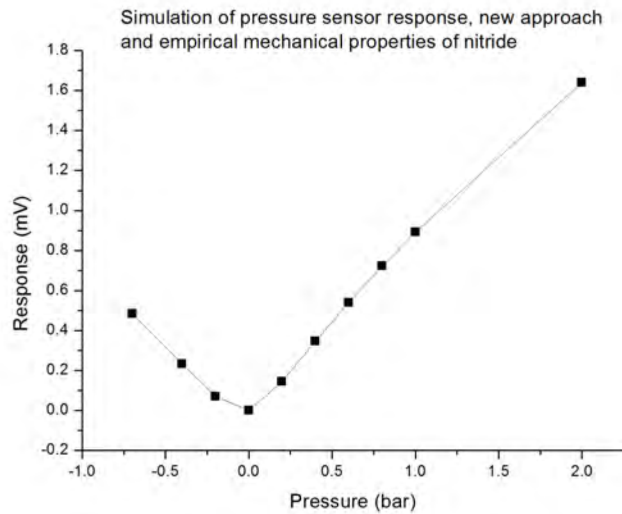

Figure 4.21: Simulation of pressure sensor response using

shown in figure 4.21, however, is very close to the result obtained when considering mean strain, the linear fit for points between 0.2 and 2 bar has a slope of 0.83 mV/bar. The approximation of mean strain would then seem to be reasonable (provided that the above

approach is okay).
The conclusion must then be, that the estimate for the gauge factor for a 100 nm gold thin film to $(1 + 3\nu)$ is too high. It should be noted though, that the thin wires between the strain gauges (seen figure 2.12c) is not accounted for in the way the calculations are done, and this will also lower the actual response a little.

4.3.8 Additional thoughts on the pressure sensor

As has been touched earlier, two effects are at play when considering strain in the gold of the pressure sensor, the edges and the large membrane. The edges are dependent on the direction of the pressure, here compression is observed for negative pressures and tension for positive ditto. On the membrane, the stress will be tensile for both pressure directions. This means that for negative pressures, these two effects must be competing and the response here must say something about the magnitude of the two effects. If first, the simulations are considered, like the plot shown in figure 4.21 it is clear that the tensile stress of the membrane "wins" -the response is roughly the same in both directions. For the experimental results however this is different, if considering figure 4.10 it is seen how a totally linear behavior around zero pressure was seen for chip1 at room temperature. Chip2 was tested very little at negative pressures, but also here the response was not the same for both pressure directions. If nothing else, this suggests that something is not taken into account in the Comsol simulations and that it is not sufficient to understand the phenomena. It could also seem that the actual response of the sensor is responding a lot more linearly than the simulations predict, and if one can spot a non linearity, it actually seems that the response is 'bending up' in the experimental results, contrary to the simulations where the slope seems to flatten.
Like AFM has been used to measure the deflection, it is also possible to imagine how this tool could be used for detailed studies of the structure and deflection profile of the membrane with gold on. With this knowledge it might be possible to better understand the phenomena and thereby perhaps improve the design even more. Should it turn out that the edges are the primary source of strain, it might be preferable to shorten the strain gauge so a higher fraction is placed close to the edge. If, on the other hand the strain out on the membrane is the primary source, the one might to avoid the edges all together, and in that way perhaps get a more reproducible result, since the magnitude of the stain will be smaller, and with that also the risk of plastic deformation of the gold.
All in all, the obtained results give no definitive answer to the mechanisms at play, but on the other hand, it is clearly shown that the sensor gives a response strong enough to be a viable pressure sensor for this application. The use of other materials with a higher gauge factor, but in a setup like the one presented here, is definitely also something worth exploring.

5
Electron Microscopy

5.1 SEM

5.1.1 A brief introduction

When the project was first started, it was the ambition to do a series of experiments in the SEM. Unfortunately the design and fabrication phases got prolonged to a degree that made this impossible. Therefore only a few simple experiments where done, and a live test of all devices working together inside the SEM was regrettably never conducted.
The experiments that were performed was first of all a live electroplating on a first generation chip that had been covered with two large gold electrodes. Secondly, nanoparticles in liquids were observed using our chip.
Before moving on to the results, a very brief introduction will be given to Scanning Electron Microscopy.

Scattering and detectors

A SEM (Scanning Electron Microscope) works by accelerating free electrons to 2-30keV toward the sample. When the sample is hit by the incoming electrons, some of these will experience an elastic collision and scatter back. These are high energy electrons, and are detected by a semiconductor crystal just above the sample, the BSED. Another effect is that the incoming electrons kicks off electrons from the sample, these are called secondary electrons, SE. SEs are low energetic electrons and are detected by a positively charged metal grid, that attracts and detects the electrons. For each pixel of the picture, the number of electrons hitting the detectors, will give information about the surface structure and the density of the material in the sample. The higher atomic number of the elements in a substance, the more electrons will be backscattered.

Penetration depth

The penetration depth of which you look into the sample is very dependent on the energy of the incoming electrons. This is very apparent when studying liquids, because the scattering on water molecules is not as strong as metal. When looking through a membrane, there will be a minimum energy that is required for the electrons to penetrate the membrane and scatter on whatever is behind it.

Charge building in the chip

It is a common problem when doing SEM experiments that charge from the incoming electrons will build up in the sample, which can lead to serious distortion of the pictures. For that reason it is desirable to be able to discharge the sample and it can be covered with an ultra thin gold layer and be connected to the ground for discharge.

5.2 Pictures from wet SEM

5.2.1 Movie of moving silver colloids in glycerol

For this experiment, a drop of glycerol was mixed with silver nanoparticles of size $\tilde{4}5$ nm and placed on a glass plate. Next, the chip was placed on the drop, membrane down, and the sides closed with nail polish.
The reason for using glycerol is that it is a very high viscosity liquid, that will slow the movement of the particles. The diffusive motion of a particle in a liquid under no external force is described by the following formula ([Nelson, 2004]):
With $\widetilde{r}$ being the distance the particle moves in time t, then

$$\widetilde{r} = \sqrt{\langle r^2 \rangle} = \sqrt{\frac{k_B T}{\pi \eta R} \cdot t} \tag{5.2.1}$$

where η is the viscosity of the liquid, R is the and radius of the particle.
If T=293K then a 45 nm particle will, in one second, move $\widetilde{r}$=7.9μm in water and $\widetilde{r}$=0.24μm in glycerol.
This means, that in water, it will be absolutely impossible to spot a 45nm particle, which will move 175 times it's own diameter per second. In glycerol, the size to movement ratio is 5.3, and here it might be possible to spot these small particles and see them move. Otherwise, if the small particles are to be used to measure the resolution of the microscope, then the particles will need to be fixed on the surface of the membrane instead.
It was however achieved to see movement, and it is shown in figure 5.1, that displays frames from a movie of the 45 nm silver particles in glycerol. Movie is found here, time indications figure 5.1 refer to this file. From the scale though, it is quickly seen that the particles must consist of many agglomerated smaller colloids. The scale of the pictures is so big, that 45 nm particles would only be seen as dust or not at all. Notice also how the particles stand out as white on the dark background, because silver is heavier atoms than what glycerol is comprised of.
Several particles are seen moving around in this sample. The motion though, appears not to be diffusive, the particles emerge, than move for a few seconds and come to a halt. The particle marked by the green arrow in the first picture is seen moving 'north' from frame 5.1a to 5.1b, then it stops. In the second frame, one can also see how a big cluster of particles appears and becomes more clear throughout the sequence. The last particle marked by a blue arrow, also moves in the vertical plane, it is seen how it seems to become more focused with time. A lot of other particles are also seen, but they are completely fixed. They seem to be stuck on the surface, which might also be what happens to the particles that are seen moving at first, but then stops. No estimate will be given on speed here.

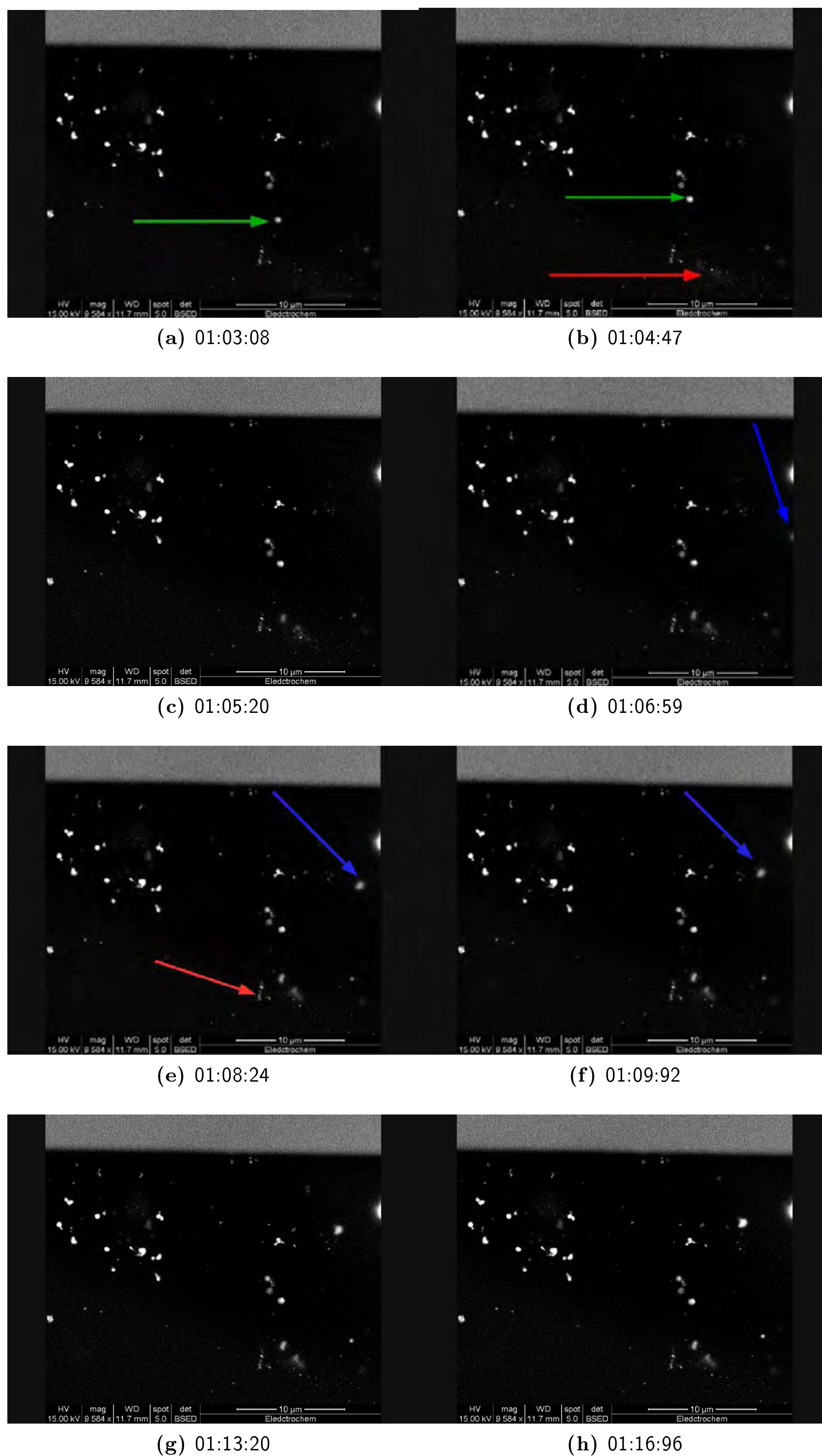

(a) 01:03:08
(b) 01:04:47
(c) 01:05:20
(d) 01:06:59
(e) 01:08:24
(f) 01:09:92
(g) 01:13:20
(h) 01:16:96

Figure 5.1: Frames from movie showing 45 nm silver particles in glycerol moving around.

5.2.2 Electroplating with gold

This experiment where done with a small 3×3mm^2 chip, that was made by Torben Hansen before this project started, but the following preparation was done by the members of this group. The chip was glued to the holder seen on figure 3.2. Then a 25μm gold wire was placed across the chip and on top of the membrane, and 100nm Au was deposited on the chip. Afterwards, the wire was removed, and two Au electrodes with a 25μm gap had been formed on the membrane.
The chip holder was filled with a solution containing gold ions, and a potential difference was set between one of the electrodes and a platinum wire also placed inside the cell. At the same time, the membrane was monitored with SEM.
This result is seen in figure 5.2 and 5.3, here it is clear that watching gold electro deposition live in SEM through the nitride membrane is possible.

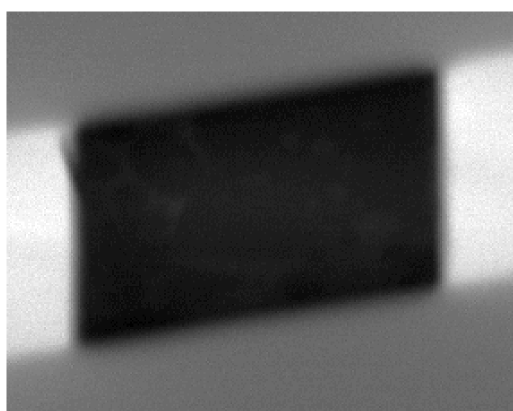

Figure 5.2: Here the two large Au electrodes on the simple chip is seen before deposition of Au.

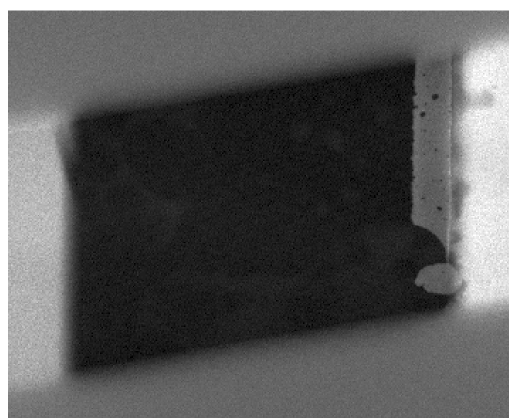

Figure 5.3: Same picture as 5.2, but here electro deposition of Au has started, an dis clearly seen.

5.2.3 Cyclic voltammetry

Now that it had been confirmed that that it was possible to see micro- and nanoparticles particles through the membrane, and that it was possible to observe electro deposition in SEM. Unfortunately it was not without problems making the electro chemistry work in our chip, there was simply no signal from the electrodes, when the chamber was filled with electrolyte. This could either be due to air bubbles on the surface, it turned out to be very difficult filling up the chip holders without getting air stuck in there, and these would then break the contact between electrode and electrolyte. Secondly, there could be residual resist on the chip, that would also block the connection.
To solve the first problem, new sample holders were made, and to remove any resist left on the chip, they were cleaned with plasma at 200 W for 10 minutes.
Electrochemistry was performed on one of these chips that was simply kept suspended in buffer solution (3 mM KH_2PO_4 (kalium di hydrogen phosphat), 3 mM $Na_3C_6H_5O_7$ (natrium citrat)), and cyclic voltammetry (C-V) was run to do a baseline measuring. When later, a chip in a cell and tested, it is known how the C-V-diagram should look like when contact is obtained. On figure 5.4 a C-V of the chip electrode 1a (turn to figure 2.18d if necessary) is connected and counter- and reference electrode are made of platinum. Later, platinum was measured vs a SCE electrode (Saturated calomel electrode, standard reference in electro chemistry), and the plot is made vs SCE. On figure 5.4 oxidation and reduction peaks are clearly seen.

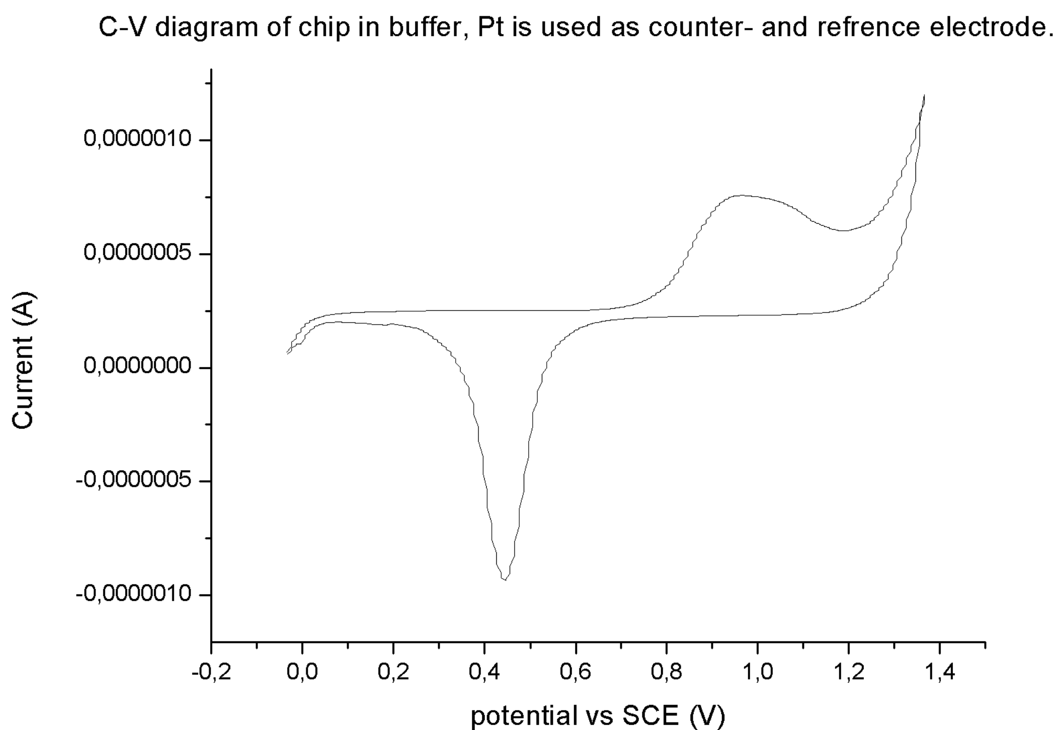

Figure 5.4: A C-V plot of Au vs Pt in buffer, 3 mM kalium di hydrogen phosphat, 3 mM natrium citrat.

It has been seen that the membrane is applicable for electron microscopy, electroplating has been done and cyclic voltammetry performed using the small electrodes of the chip. Clearly, if the problems of making contact to the chip were solved (which should be very possible), doing a full test, using all sub-devices inside the SEM should not be too far off.

6
Outlook and Conclusion

6.1 Future work

6.1.1 The design

The biggest issue with respect to the sub-devices has been the pressure sensor. The results seem promising, but there is still much lack of understanding as to exactly how it works. A big consideration has been the edges, and if the strain here, maybe becomes large enough to permanently deform the gold, and therefore move the offset between measurements. On the other hand, if the edges give the major contribution to resistance change, then these should still be included in the design.
Something that is no doubt about though, is that in our design, too large a fraction of the strain gauge resistor is not subject to strain, we therefore propose a new design shown in figure 6.1. Here the transverse wires are placed with as small a gap as possible to place as much resistance as possible here. Would it be concluded that the edges are important, then the wires could be stretched to cover these, but they should stop right at the edge and not continue 5 μm out on the chip. Here, instead of placing the two strain gauges opposite,

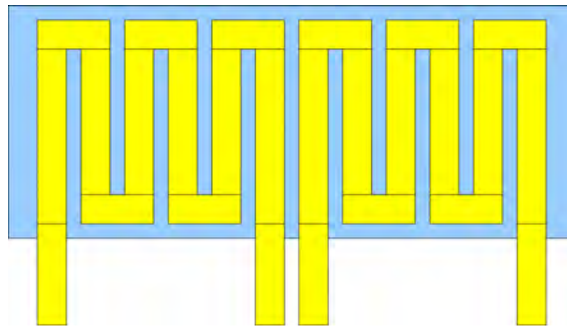

Figure 6.1: Sketch of a design for pressure sensor, where edge effect are tried removed.

they would be placed next to each other for maximum utilization of the membrane strain. As stated before, trying other materials would also be very interesting. An unsuccessful attempt was made with platinum during this project, but most of the membranes broke, possibly because of stress in the platinum, maybe because of bad luck. It was also discussed to try a titanium/tungsten alloy, for which process parameters giving zero stress has been developed here at Nanotech.

6.1.2 Electrodes

Unfortunately the design of the electrodes was not properly discussed with Palle inthe design phase, and therefore it did not become optimum. It was clear that electrodes should be placed with varying gaps, which was done, 3, 6, and 9 micron. What was not done was

to create a proper counter electrode. Preferably this would have an area much larger than the small working electrodes, and a big plate of gold placed next to the thermistor would have been perfect. One reason here is that when doing electroplating, a supply of gold ions is needed, something that could come from a big electrode like that. Still, an external electrode not on the chip can be used but this might have been an idea. Furthermore, a mask should be made to add another lithography step. Here, the entire chip should be covered with an insulator, except the pressure sensor, that has to be able to deflect freely, and the very tip of the small electrodes. One reason for this is, that when doing plating an electrode, it will be done on the entire exposed area of it. This has been considered in the design, the distance between electrodes is everywhere larger than the gap between the tips, but still complete shielding would be the best.

6.1.3 Transfer to TEM

A liquid TEM would require two chips with membranes places very close to each other, most likely no more than a few hundred nanometers or possibly less. This also means that the membranes could not be allowed to deflect, and they either had to be very small, meaning possible alignment problems, or the membranes could be 'glued' together leaving only a narrow channel into which the electrodes should be exposed and liquids and gases could pass. The pressure sensor though, would have to be connected to this channel to measure pressure, but meanwhile the membrane should be able to move freely.

6.2 Conclusion

As stated by our supervisor, this has been a true "‘engineer's assignment"’. A set of requirement was set up: Produce a MEMS device with membrane, electrodes, temperature- and pressure sensors and internal heating. The process has included design, with the use of analytical calculations, simulations and estimates, together with search for relevant literature. There has been fabrication in the Danchip cleanroom, involving training in, and hands on experience with, relevant machines and processes. When the devices where finally produced, they were tested and calibrated in a controlled test environment. Finally, a peek was taken into the world of electron microscopy.
With background in fundamental equations and simple simulations, a design was proposed and the chip was fabricated. When the device was finished, all sub-devices were tested, to see if the intended specifications were obtained. For both thermistor, heater and pressure sensor, the overall goal was obtained, they were by and large working as intended.
There were clear discrepancies from the designed specifications though, and where necessary, additional theory and simulations have been added. Explaining the behavior of the pressure sensor though, has not been complete, but an attempt has been made to expand the theory and point in which direction to take further experiments. Furthermore, AFM was shown to be an effective tool in characterization of the membrane.
It is our hope that this work will provide a sound foundation for the future of this research field here at DTU Nanotech.

Bibliography

S. Thiberge, O. Zik, and E. Moses. An apparatus for imaging liquids, cells, andother wet samples in the scanning electron microscopy. *Review of Scientific Instruments*, 2004.

J.F. Creemer, S. Helveg, G.H Hoveling, S. Ullmann, A.M Molenbroek, P.M Sarro, and H.W. Zandenbergen. Atomic-scale electron microscopy at ambient pressure. *Ultramicroscopy*, 2008.

Á. Kovács, A. Kovács b, and U. Mescheder. Estimation of elasticity modulus and fracture strength of thin perforated sin membranes with finite element simulations. *Computational Materials Science*, 2007.

R.L. Edwards, G. Coles, and Jr W.N. Sharpe. Comparison of tensile and bulge tests for thin-film silicon nitride. *Society for Experimental Mechanics*, 2004.

Scott D. Collins. Etch stop techniques for micromachining. *Journal of The Electrochemical society*, 1997.

Warren C. Young and Richard G. Budynas. *Roarks Formulas for Stress and Strain.* 2002.

Jinling Yang and Oliver Paul. Future properties of lpcvd silicon nitride thin films from the load-deflection of long membranes. *Sensors and actuators*, 2002.

Erik V. Thomsen and Jacob Richter. Piezo resistive mems devices: Theory and applications. Note supplied for a course in MEMS-fabrication here at DTU, 2007.

R.L Parker and A. Krinsky. Electrical resistance-strain characteristics of thin evaporated metal films. *Journal of Applied Physics*, 1963.

S.U. Jen, C.C. Yu, C.H. Liu, and G.Y Lee. Piezoresistance and electrical resistivity of pd, au, and cu films. *Thin Solid Films*, 2003.

CRC. *CRC Handbook of Chemistry and Physics.* CRC Press, 2008.

Resistivity, wikipedia article. URL http://en.wikipedia.org/wiki/Resistivity. Numbers are referenced from "'Principles of Physics (2nd ed ed.)"'.

Warren C. Young and Richard G. Budynas. *Intoduction to Solid State Physics.* Wiley, 2005.

O.S Heavens. *Thin Film Physics.* Methuen & CO, 1973.

Philip Nelson. *Biological Physics.* FREEMAN, 2004.

Volker Ziebart, Oliver Paul, Ulrich Münch, Jürg Schwizer, and Henry Baltes. Mechanical properties of thin films from the load deflection of long clamped plates. *Journal of Microelectromechanical Systems*, 1998.

7
Appendix

APPENDIX 1

Summary of the model for large deflections of membranes

Primary reference on this is [Yang and Paul, 2002] but the model is first presented by [Ziebart et al., 1998]

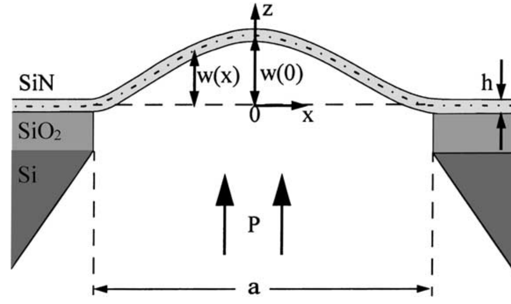

Figure 7.1: Membrane of width a deflected under pressure P, profile according to function $w(x)$. Neutral fiber marked with dashed line. (property of [Yang and Paul, 2002])

Plane-strain modulus $E_{ps} = E/(1-\nu^2)$ is introduced, where E is Young's modulus and ν is Poisson's ratio
The deflection profile in the middle section of the membrane is governed by the function $w(x)$, where x-axis is zero in the middle of the membrane. s denotes the in-plane stress in the neutral fiber (see figure 7.1) when the membrane is loaded, P is the pressure on the membrane and s_0 is prestress in the material. All coordinates are transformed into reduced dimensionless form:

$$\bar{s} = s(a/h)^2/E_{ps} \tag{A1-1}$$
$$\bar{s_0} = s_0(a/h)^2/E_{ps} \tag{A1-2}$$
$$\bar{P} = P(a/h)^4/Eps \tag{A1-3}$$
$$\bar{w} = w/h \tag{A1-4}$$
$$\bar{x} = x/a \tag{A1-5}$$

If the effective stress is $\bar{s}$ then

$$\bar{w}(\bar{s},\bar{x}) = \bar{P}G(\bar{s},\bar{x} \tag{A1-6}$$

where

$$G(\bar{s},\bar{x}) = \frac{1}{2\bar{s}}\left(\frac{1}{4}-\bar{x}\right) - \frac{cosh(\sqrt{3\bar{s}}) - cosh(2\bar{x}\sqrt{3\bar{s}})}{4\sqrt{3\bar{s}^3}sinh(\sqrt{3\bar{s}})} \tag{A1-7}$$

The in-plane stress $\bar{s}$ is related to the max deflection $w_0 = w(\bar{s}, 0)$ and the prestress as:

$$\bar{s} \quad = \quad \bar{s}_0 + \frac{1}{2} \cdot \bar{w}_0^2 \cdot H(\bar{s}) \qquad \text{(A1-8)}$$

where

$$H(\bar{s} = \frac{4((8+4\bar{s})sinh(\sqrt{3\bar{s}})^2 - 6\bar{s} - 3\sqrt{3\bar{s}}sinh(2\sqrt{3\bar{s}}))}{(\sqrt{3\bar{s}}sinh(\sqrt{3\bar{s}}) - 4sinh(\sqrt{3\bar{s}}/s)^2)^2} \qquad \text{(A1-9)}$$

APPENDIX 2

Matlab code listing, fit of large deflection model to measured values.

fitmem.m

```
clear
clf

width=50e-6;
h=50e-9;
P_afm=[0,0.037,0.076,0.1069,0.1431,0.468,0.8188,1.156,1.525,1.865,2.5892,2.844,3.209,5.6];
w0_afm=[0,0.05867,0.14633,0.29667,0.38067,0.82233,1.11933,1.35633,1.529,1.667,1.95933,2.014,2.1
P_COMSOL=[0.1,0.3,0.5,0.7,1.5,3.0,4.0];
w0_COMSOL=[0.2277,0.5882,0.8389,1.027,1.522,2.063,2.319];



plot(P_afm,w0_afm,'ro'); hold on;
plot(P_COMSOL,w0_COMSOL,'+'); hold on;
title('Measured deflections and model fit');
xlabel('Pressure [bar]');
ylabel('Deflection [um]');


start_fmin=[100e6,255e9];
[Estimates,error]=fminsearch(@(x) fitfun(x,P_afm,w0_afm,h,width),start_fmin);


Eps=Estimates(2)/(1-0.23^2);
s0bar=Estimates(1)*(width/h)^2/Eps;
P_vec=linspace(0,max(P_afm),100);
length=length(P_vec);
for i=1:length
    Pbar=P_vec(i)*1e5*(width/h)^4/Eps;
    sbar_solved=fsolve(@(x) funs2(x,s0bar,Pbar),1000);
    w0_model(i)=Pbar*G(sbar_solved)*h*1e6;
    w0_model(i);
end
plot(P_vec,w0_model);
legend('Measured value','Comsol', 'Model fit', 'Location','NorthWest');

Estimates(1)

Estimates(2)

error
```

fitfun.m

```
function error=fitfun(param,P,w0,h,width)
s0=param(1);
Eps=param(2)/(1-0.23^2);
s0bar=s0*(width/h)^2/Eps;

lengthP=length(P);
err=0;
for i=1:lengthP
Pbar=P(i)*1e5*(width/h)^4/Eps;
w0bar=w0(i)*1e-6/h;
start_solve=s0bar+w0bar^2*3.14^2/4;
sbar_sol=fsolve(@(x) funs(x,s0bar,w0bar),start_solve);
err=err+(Pbar*G(sbar_sol)*h*1e6-w0(i))^2;
end
error=err;

end
```

funs.m

```
    function sbarfun=funs(sbar,s0bar,w0bar)
    sbarfun=-sbar+s0bar+1/2*w0bar^2*H(sbar);
    end
```

G.m

```
function out=G(sbar_sol)
out=(1/(2*sbar_sol)*(1/4)-(cosh(sqrt(3*sbar_sol))-1)/(4*sqrt(3*sbar_sol^3)*sinh(sqrt(3*sbar_sol
end
```

H.m

```
function out=H(sbar)
out=(4*((8+4*sbar)*sinh(sqrt(3*sbar))^2-6*sbar-3*sqrt(3*sbar)*sinh(2*sqrt(3*sbar)))/((sqrt(3*sb
end
```

Appendix 3

		Machine	Process parameters	Comments
1.1	Wafer, n-type, 350um double polished			
	LPCVD, low stress nitride, 75nm			
1.2	LPCVD nitride	Nitride oven	Recipe: Sirich DSC:85sccm,NH3:21sccm,112torr,835degC,15 min	
	Inspection	Filmtek	Nitride program	Result:
	Photolithography Mask 1, negative process			
2.1	HDMS	HDMS oven		
2.2	Spin on photoresist, backside, 1.5um	KS spinner	AZ5214E (Danchip_4_6_1.5)	KS Spinner Needed due to gentle handling
2.3	Bake	90 deg/C hotplate	Time: 90 s	
2.4	Alignment and exposure	KS aligner	Exposure time: 3 s (CI2 Intensity: 7)	
2.5	Reverse bake	120 deg/C Hotplate	Time: 120 s	
2.6	Flood exposure	KS aligner	Exposure time: 30 s	
2.7	Devoloper		Time 75 sec (Took 2 min to develop last time)	Visually control that it is fully developed
	RIE to remove nitride			
3.1	RIE etching, backside	RIE 1	Recipe: TMHNITR2 Time: 3.5 min	
3.2	Remove resist with plasma		Time: 10 min	Alternatively, strip resist in acetone
	KOH			
4.1	HF to remove oxide		30 sec.	
4.2	KOH to etch all Si	KOH2	80 degC Ca. 4h. 30min /through	

	Photolithography Mask 2, negative process			
5.1	HDMS	HDMS oven		
5.2	Spin on photoresist, frontside, 1.5um	KS spinner	AZ5214E (Danchip_4_6_1.5)	
5.3	Bake	90 deg/C hotplate	Time: 90 s	
5.4	Alignment and exposure	KS aligner	Exposure time: 3 s (CI2 Intensity: 7)	
5.5	Reverse bake	120 deg/C Hotplate	Time: 120 s	
5.6	Flood exposure	KS aligner	Exposure time: 30 s	
5.7	Devoloper		Time 75-120 sec	
	Metal deposition			
6.1	Metal deposition	Alcatel	(Cr/Ti)-Au	10 nm + 50 nm
6.2	Lift off	Lift off bath		
	Spin on photoresist, frontside, 9.5um			
	Spin on photoresist, frontside, 9.5um	KS spinner		Manually apply resist
7.1	Bake on hotplate	90 deg/C Hotplate	Time: 2 min	
7.2	**Saw wafer**			